Fundamentals for remote structural health monitoring of wind turbine blades - a preproject. Annex E. Full-scale test of wind turbine blade, using sensors and NDT

Kristensen, O.J.D.; McGugan, Malcolm; Sendrup, P.; Rheinländer, J.; Rusborg, J.; Hansen, A.M.; Debel, C.P.; Sørensen, Bent F.

Publication date:
2002

Document Version
Publisher's PDF, also known as Version of record

Risø-R-1333(EN)

RISØ

Fundamentals for Remote Structural Health Monitoring of Wind Turbine Blades – a Preproject

Annex E – Full-Scale Test of Wind Turbine Blade, Using Sensors and NDT

Ole J.D. Kristensen, Malcolm McGugan, Peter Sendrup, Jørgen Rheinländer, Jens Rusborg, Anders M. Hansen, Christian P. Debel and Bent F. Sørensen

Risø National Laboratory, Roskilde, Denmark
May 2002

Abstract A 19.1 metre wind turbine blade was subjected to static tests. The purpose of the test series was to verify the abilities of different types of sensors to detect damage in wind turbine blades.

Prior to each of the static test-series an artificial damage was made on the blade. The damage made for each test-series was surveyed during each series by acoustic emission, fiber optic micro bend displacement transducers and strain gauges. The propagation of the damage was determined by use of ultra sonic and X-ray surveillance during stops in the test-series.

By use of acoustic emission it was possible to detetct damage propagation before the propagation was of visible size. By use of fiber optic micro bend displacement transducers and strain gauges it was possible to measure minor damage propagation.

By use of both ultra sonic, and X-ray NDT-equipment it were possible to determine the size of propagated damage.

ISBN 87-550-3034-3
ISBN 87-550-3035-1 (Internet)
ISSN 0106-2840

Print: Pitney Bowes Management Services Denmark A/S, 2002

Contents

1 Introduction

As part of the PSO-project "Grundlag for fjernovervågning af vindmøllevingers tilstand (Fase I: Forprojekt)", supported by PSO-funding through Elkraft System, contract no. Bro-91.055, FU nr. 1102, a 19.1 metre wind turbine blade provided by LM Glasfiber A/S has been undergoing a static test.

The test was carried out in collaboration between the following participants:

LM Glasfiber A/S (Providing blade for testing)
FORCE Technology (Ultrasonic determination of damage propagation)
DELTA (Development of, and measurements with optic micro bend displacement transducers)
Innospexion (X-ray determination of damage propagation)
Sensor Technology Center A/S (Cost-benefit analysis and consultancy on sensors)
Risø National Laboratory (Lab.-tests and measurements)

The purpose of the test series was to verify the abilities of different types of sensors to detect damage on wind turbine blades. Furthermore, the purpose of the test was to evaluate different types of NDT-tests in means of predicting the propagation of damages.

Prior to each of the static test-series an artificial damage was made on the blade. Two types of damages were chosen for the test. The first damage (damage no. 1) was a notch in the trailing edge, this damage was expected to propagate either in longitudinal direction of the blade or keep propagating in the direction of the crack. The second (damage no. 2) was a failure in the glued joint in the trailing edge. This damage was expected to propagate in the trailing edge with an increase in the area of damaged glue. Both damages were made artificial by use of an angular grinder. The damage types represented here are classical examples of possible defects, which can evolve, in composite structures including wind turbine blades.

The damages were surveyed during each test-series by acoustic emission and strain gauges. For the second series fiber optic micro bend displacement transducers were imbedded in the blade for an additional surveillance of the damage. In addition to the sensor surveillance of the blade during test, video cameras were positioned to inspect the blade and damage under test. The propagation of the damage was determined by use of ultra sonic and X-ray surveillance during stops in the test-series. During these stops still-photos were taken to verify the visible size of damage.

The main report of the project is: "Fundamentals for remote structural health monitoring of wind turbine blades - a pre-project", Bent F. Sørensen, Lars Lading, Peter Sendrup, Malcolm McGugan, Christian P. Debel, Ole J. D. Kristensen, Gunner Larsen, Anders M. Hansen, Jørgen Rheinländer, Jens Rusborg and Jørgen D. Vestergaard, Risø-R-1336(EN), May 2002.

2 Blade geometry definitions

Distances on the blade and forces applied to the blade are related to the blade as indicated in 0.

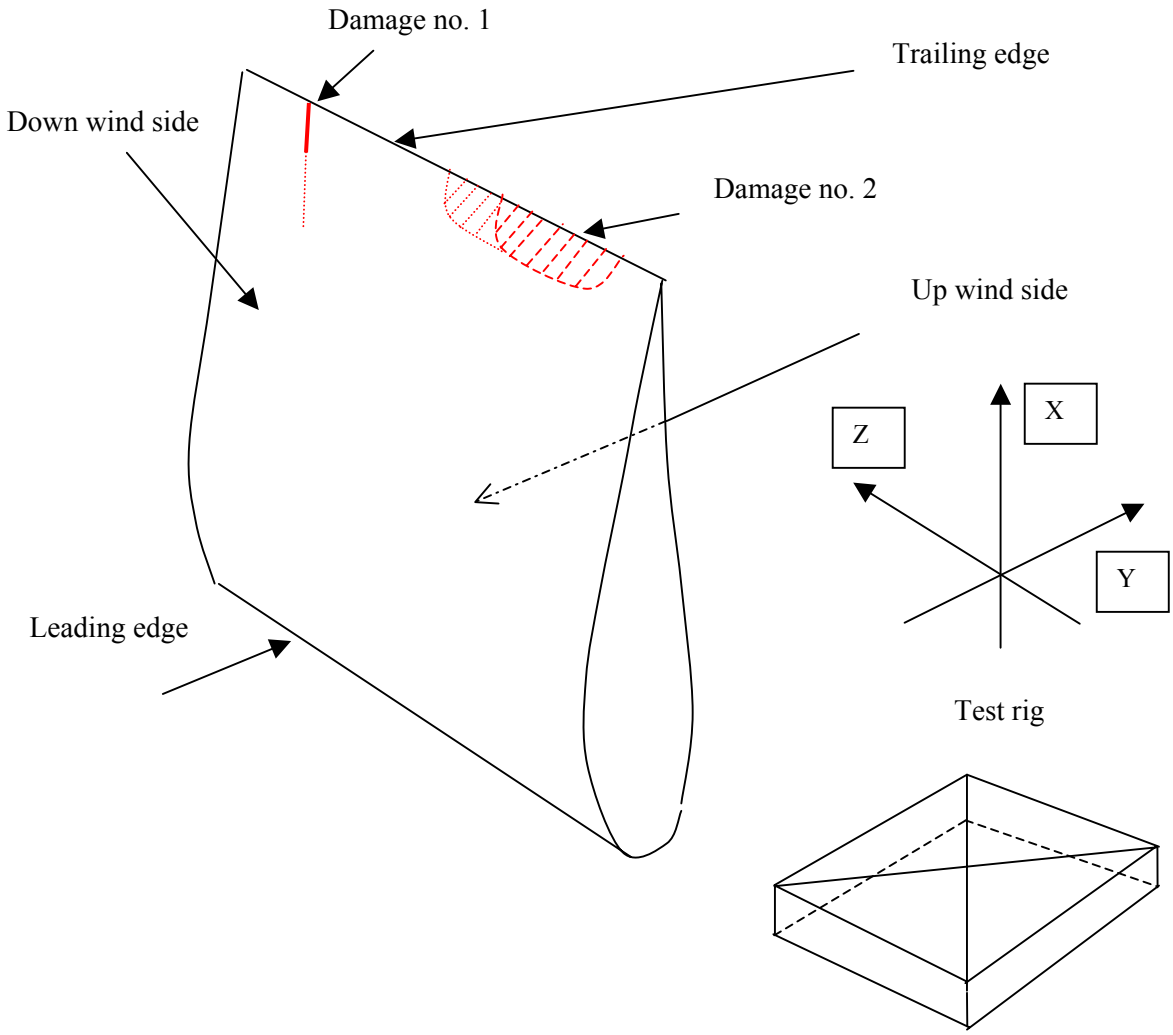

Figure 1. Sketch with the definitions that are used in this report

3 Estimates of load requirements

In this section we estimate the load levels that are necessary to cause growth of cracks from the artificial damages. The models are rather simple, and the blade tests do not rigorously conform to the assumptions of the models. However, we only use the models to provide an order of magnitude of the load level required to propagate the damage.

3.1 Notch in laminate at trailing edge, damage no. 1

The loading and damage type is shown schematically in Figure 2. The applied force, P, is positioned a distance ℓ from the damage. The force creates a bending moment, M, which at the damaged site, is given by

$$M = P\ell \tag{1}$$

The damage is in the form of a cut, which acts as a pre-existing crack. The crack length is denoted a. Thus, the problem can be considered being the propagation of a crack in a plate that is subjected to bending, see Figure 2. This is analysed by a fracture mechanics model. According to the fracture mechanics model, the crack tip stress intensity factor is [Ref. 2]

$$K_I = \sigma_{\max}\sqrt{\pi a}\, f(a/W) \tag{2}$$

where

$$\sigma_{\max} = 6\frac{M}{BW^2} \tag{3}$$

is the nominal maximum stress generated by the bending moment, B is the thickness of the plate and W is the width of the plate (see Figure 2). The function f is a non-linear, but dimensionless function of the ratio between crack length and plate width, a/W. The energy release rate G can be estimated from (assuming plane stress state and isotropic elastic properties)

$$G = \frac{K^2}{E} \tag{4}$$

where E is the Young's modulus of the material. Cracking is assumed to occur when the energy release rate equals a critical value, the fracture energy G_c:

$$G = G_c \tag{5}$$

We now proceed to use the model. The damage is positioned at z = 14.5 m (z being the distance from the root), and the force is positioned at z = 16.3 m. Thus, the moment arm becomes ℓ = 16.3 m - 14.5 m = 1.8 m. The nominal maximum applied force, P, is 31.8 kN. Then, by (1) we estimate $M = 55.8 \times 10^3$ Nm. Assuming the length of the pre-cut crack, a, to be 0.1 m and W = 1 m, we get [Ref. 2] $f(a/W = 0.1) = 1.0$. Assuming B = 0.01 m (corresponding to the thickness at of the blade at the tip of the pre-crack) we get by (3) $\sigma_{\max}$ = 33.5

MPa, and by (2) K_I = 18.8 MPam^{½}. Assuming E = 30 GPa we get by (4) G = 11.7 kJ/m^2. Thus, crack growth will take place if the fracture energy is less than 11.7 kJ/m^2.

The fracture energy of the blade blade material, G_c, has not been measured, but it is expected to be in the order of 2-5 kJ/m^2. Thus, the pre-cut length and load level generates an energy release rate that does exceed the expected fracture energy. Consequently, crack growth of the pre-cut is expected at the suggested load level.

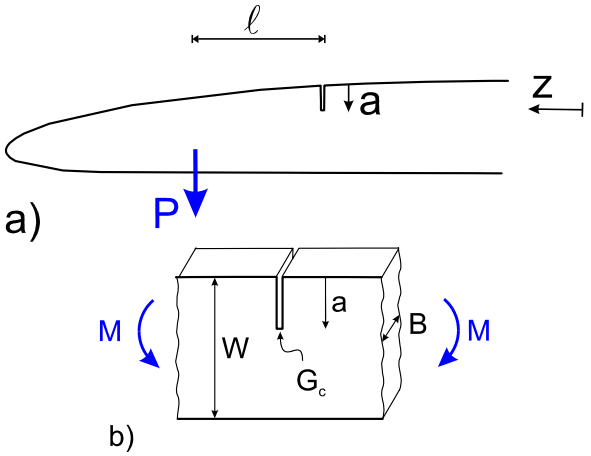

Figure 2. Sketch of the loading and damage type 1: (a) The applied force, P*, creates a bending moment. (b) The damage progression is modelled by the growth of a crack in a plate subjected to a bending moment.*

3.2 Adhesive failure at trailing edge, damage no. 2

The second type of damage, failure of an adhesive joint, is created by removing the adhesive layer at the trailing edge. In the following we estimate how large the artificial damage should be (adhesive-free length) and how high the applied loads are expected to be.

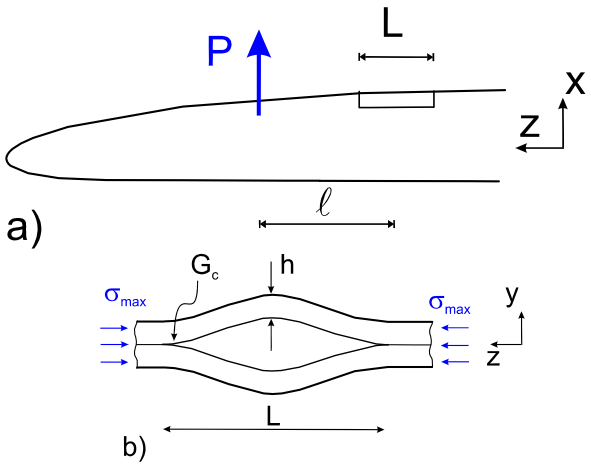

Figure 3. Sketch of the model for Test 2. The adhesive is removed over a length, L*, along the trailing edge (a). The maximum axial stress must be so high that buckling occurs and the energy release rate must be equal to the fracture energy,* G_c*, of the adhesive.*

The intended failure mode is buckling-driven cracking of the adhesive. Thus, we must ensure that the adhesive-free length, *L*, is sufficiently long to ensure both *local buckling* and *crack growth*. The load is applied somewhat similar to the loading in Test 1, except that now the force pulls upwards, creating compression stress in the axial direction near the trailing edge, see Figure 3.

Buckling of the skin in the adhesive-free region happens when the axial stress reaches a critical value given by [Ref. 3]

$$\sigma_c = \frac{\pi^2}{3}\frac{E}{1-\nu^2}\left(\frac{h}{L}\right)^2 \tag{6}$$

where E is the Young's modulus, ν is the Poisson's ratio, h is the thickness of the laminate (a more accurate estimate for the onset of buckling is obtained by finite element simulation, see paragraph 3.3).

Buckling-driven cracking of the adhesive is assumed to happen when the energy release rate of this failure mode, G, exceeds a critical value equal to the fracture energy of the adhesive, G_c. The energy release rate of this failure mode is well approximated by [Ref. 3]

$$G \approx 1.2\frac{1-\nu^2}{2E}\sigma_{max}^2 h \tag{7}$$

We are now ready to use the model. Using equation (6) with E = 30 GPa, ν = 0.3, h = 5 mm, L = 300 mm we get σ_c = 27 MPa. The damage is positioned at z = 11.0 m, and the force is positioned at z = 13.1 m. Thus, the moment arm becomes ℓ = 2.1 m. The nominal maximum applied force, P, is 58 kN. By (1) we estimate M = 122 x 10^3 Nm. From (3) this bending moment give a maximum compressive stress σ_{max} = 73 MPa. This value is higher than the 27 MPa calculated for the critical buckling stress, σ_c. Thus, the load level is sufficiently high

to cause buckling. To assess whether adhesive failure will occur, we insert σ_{max} into (7), which gives $G = 485$ J/m^2. The fracture energy of the adhesive has not been measured, but it is expected to be in the range of 200-500 J/m^2. Thus, the energy release rate is most likely to be higher than the fracture energy ($G \geq G_c$) so that crack growth in the adhesive is expected.

3.3 Estimation of buckling load by FEM

In this project an optical sensor is to be tested. The aim of the sensor is to identify failure of the glue connection at the trailing edge of the blade. The sensor measures the distance between the upper and lower part of the trailing edge and is mounted inside the glue connection. A part of the glue connection on one of the sides of the sensor is removed – this part is referred to as the damage extent. When the blade is loaded in such a way that the trailing edge is in compression the upper and/or lower part of the trailing edge buckles and (hopefully) a crack is initiated in direction of the sensor. The present analysis is to estimate how much of the glue connection which has to be removed in order to ensure the occurrence of buckling.

During the experiment the blade is loaded at Z=9.5 m with a force of 80 kN and the blade is supported at Z=13.1m. It is expected that the reaction will be 48 kN at the supported position.

A finite element model (FEM) of the piece of the blade from Z=9m to Z=13m is modelled with the programme ANSYS. The centre of the damage, i.e. the centre of the part of the connection between the upper and lower skin which has been removed, is located at Z=11m. The section is fixed at Z=9m and is loaded at Z=13m with a force of 50.4kN in the edge direction. The result of this loading is a bending moment at Z=11m equal to the experimental set-up described above. The model is shown in Figure 4.

A macro for ANSYS was written in which the extent of the damage and the skin thickness can be varied easily. For a series of different thicknesses and damage extents buckling load is calculated and tabulated, see Table 1. (See table caption for explanation of results)

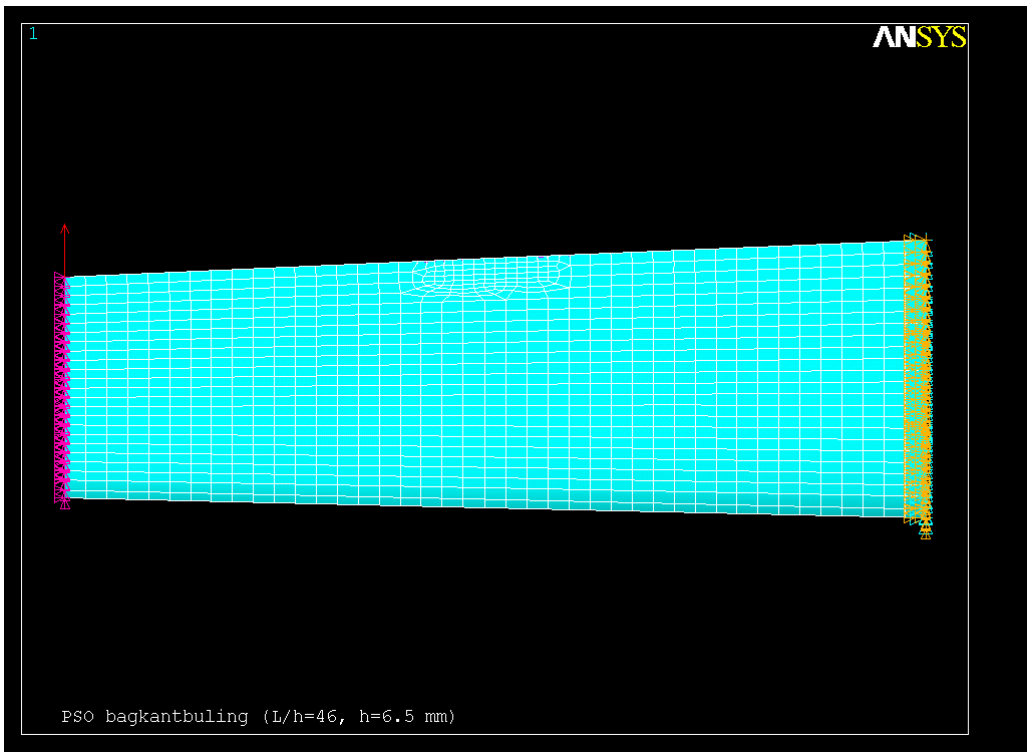

Figure 4. Example of FEM model of the blade section.

*Table 1. Load factor at buckling as function of skin thickness (h (columns)) and normalised damage extent (L/h (rows)). E.g., if skin thickness h=10mm and damage extent L=300mm then L/h=300/10=30 and then buckling occurs when the reaction force at z=13.1m is P=1.98*48kN.*

	h=10mm	**8mm**	**6.5mm**	**6mm**	**4mm**
L/h=30	1.98	1.82	-	1.66	1.35
40	1.62	1.47	-	1.26	1.06
46	-	-	1.20	-	-
50	1.43	1.31	-	1.10	0.81
60	1.36	1.24	1.08	1.01	0.68
70	-	-	1.06	-	-
80	-	-	1.06	-	-

The suggested value of damage extent is 300mm and skin thickness is estimated to h=6.5mm. This gives L/h=46 and buckling is expected to occur at P=1.20*48kN (reaction force at Z=13.1m). The buckling mode for these values is shown in Figure 5.

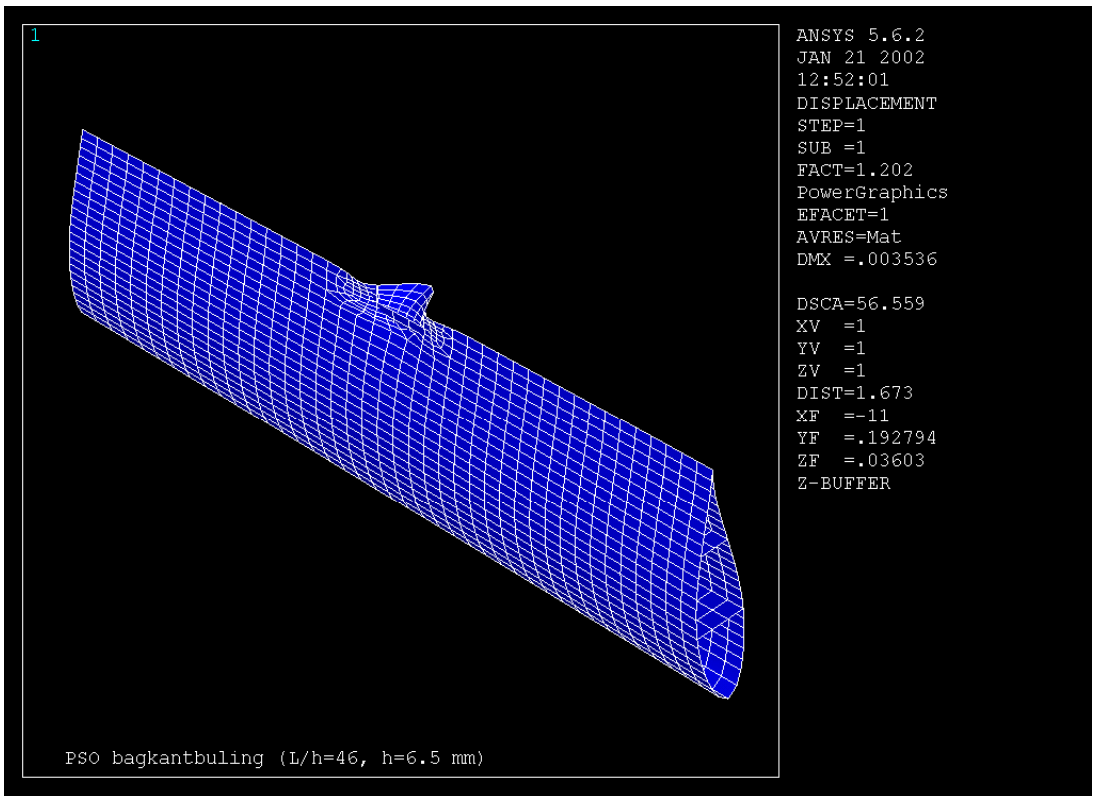

Figure 5. Buckling mode for L/h=46 and h=6.5 mm.

3.4 Remarks

From 0 it is noticed that the buckling load does not decrease significantly when L/h is increased at h=6.5mm=constant. This is because buckling involves a larger and larger part of the blade towards the leading edge of the blade, i.e. buckling is no more localised near the trailing edge. Therefore we might experience that the blade does not buckle even though the damage extent is increased and we might consider to decrease the thickness of the skin instead.

4 Experimental procedures

4.1 General testing and monitoring procedures

The test was carried out in two test series, both series were carried out in edge-wise direction. The purposes of the test series were to verify the possibilities of different surveillance sensors, and different damage determination methods. The intensions were to apply a load, which causes a local bending moment of size equal to the bending moment applied to this blade type at the type approval test, alternatively a load that causes the artificial damages to propagate. Each test-series was stopped every time a certain, not pre-desired, propagation in the artificial damage has happened. At these stops the blade was unloaded to a certain level and at this level NDT-inspections were carried out with both ultra sonic and X-ray. After NDT-inspections the load was re-applied till further propagation in damage was reached. This loading-unloading cycle was carried out repeatedly with an increasing load-level until a satisfactory result in damage-surveillance was achieved.

The applied load and the resulting deflection of the blade were measured in intervals of five seconds during all test-repetitions. Subsequent to each repetition of the tests NDT-inspections of the blade were made.

To create a basis for the NDT-inspections, both ultra sonic and X-ray inspections were made on the undamaged blade as it was received at the test-lab. When the blade was mounted in the test-rig and these initial inspections were made, the first artificial damage was made on the blade. Another NDT-inspection of the area with the artificial damage was made before testing of each of the two damages.

Real-time surveillances of the damages were made for each test-series by acoustic emission, optical micro bend displacement transducers (only damage no. 2) and strain gauges. In addition to the sensors, two videocassette recorders (VCR) were used to survey both up-wind and down-wind surfaces of the blade. The propagation of the damage was determined by use of ultra sonic and X-ray surveillance during the stops in the test-series. Along with the NDT-inspections still-photos were made of the propagated damage.

All the tests are described with name, date and duration in Table 2.

Table 2. Name and time for the individual tests

	Test-no.	**Time of start, videotape**	**Time of start**
Damage no. 1	WING001	0h 05m - 00h 11min	15/1/02 kl. 16.26
	WING002 (cancelled)	0h 13m	
	WING003	0h 23m 30s	15/1/02 kl. 18.06
	WING004	0h 31m 46s	16/1/02 kl. 08.35
	WING005	0h 51m 03s	16/1/02 kl. 10.15
	WING006	1h 21m 00s	16/1/02 kl. 12.11
	WING007 (cancelled)	1h 49m 05s	
	WING008	1h 57m 01 s	16/1/02 kl. 14.56
Damage no. 2	WING101	?	23/1/02 kl. 14.15
	WING102	?	23/1/02 kl. 15.00
	WING103	?	23/1/02 kl. 16.15
	WING104		23/1/02 kl. 16.30
	WING105	1h 38m	24/1/02 kl. 10.10
	WING106	1h 49m	24/1/02 kl. 11.15
	WING107	2h 00m (label); 2h 03m (loading)	24/1/02 kl. 13.28
	WING108	2h 28m	24/1/02 kl. 14.35
	WING109	2h 52m	24/1/02 ca. 15.25
	WING110	3h 05m	24/1/02 ca. 15.45
	WING111	3h 15m	24/1/02 ca. 16.03
	WING112	3h 28m	24/1/02 kl. 16.35
	WING113	0h 00m (new tape!)	24/1/02 kl. 17.42
	WING114	0h 29m	25/1/02 kl. 09.31
	WING115	0h 59m	25/1/02 kl. 11.15
	WING116	1h 30m	25/1/02 kl. 12.14
	WING117	1h 51m	25/1/02 kl. 12.53
	WING118	2h 14m	25/1/02 kl. 14.30

Subsequent to the testing of the blade post-mortem sectioning was made of the interesting parts of the blade. Further visual inspections of these parts were made and an additional X-ray inspection was made of the area of damage 1.

4.2 Creating notch in laminate at trailing edge

The first damage was a notch in the trailing edge of the blade. An angular grinder was used to make this notch. The depth of the notch was pre-decided to have the same size as the glue in the joint in the trailing edge.

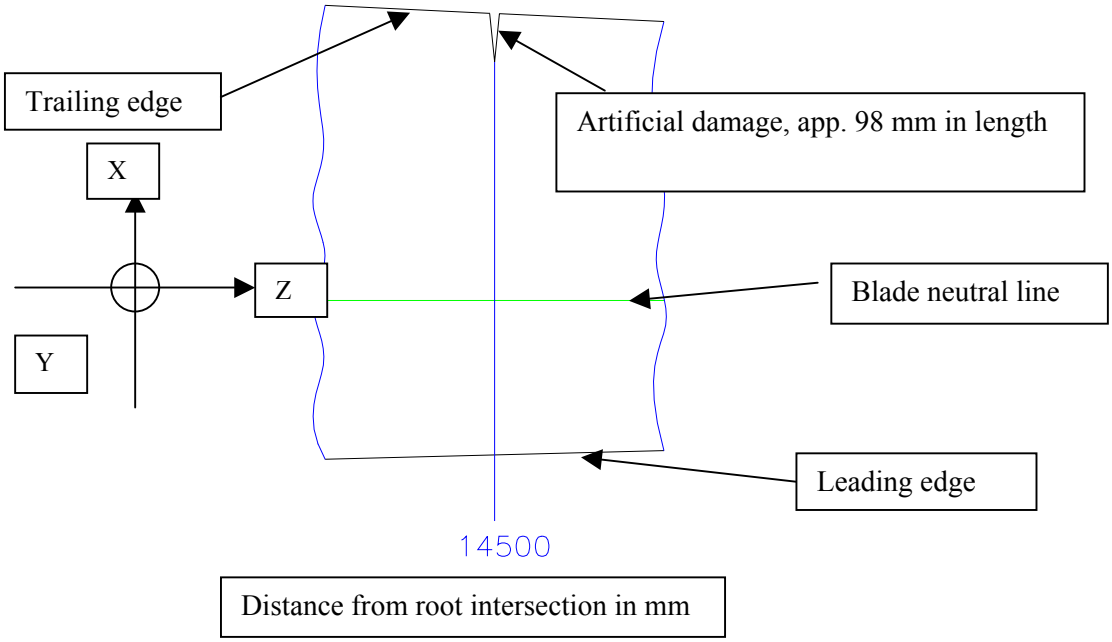

Figure 6. Position of damage for test-series 1. Up-wind surface of blade.

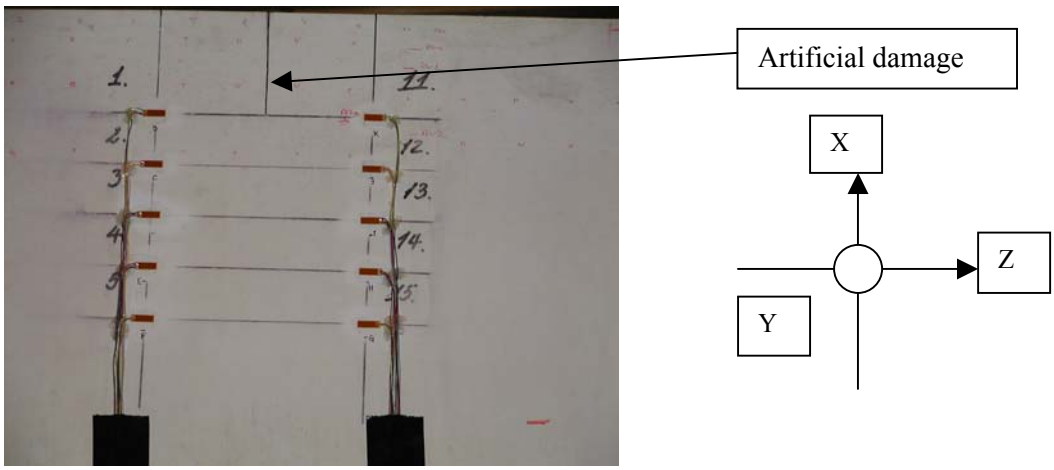

Figure 7. Up-wind surface of blade, damage no. 1. Tip-end direction to the right.

The size of the initial damage was determined to 98 mm and ended just before the line of the two strain gauges closest to the trailing edge, see Figure 6 and Figure 7. The SG numbering is made as lowest numbers on up-wind surface, and lowest numbers nearest to the root intersection.

4.3 Loading procedure and history

To make the damage propagate, load was applied further towards the tip than the damage. The load was applied downwards to create tension in the trailing edge. To prevent the part of the blade closer to the root intersection than the artificial damage from being overloaded a support was applied to the blade.

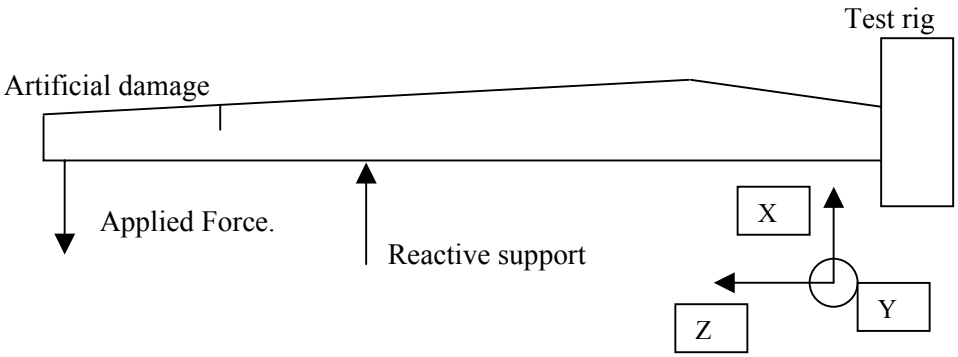

Figure 8. Principal sketch of test set-up and applied load and reactive support.

The position of the load was 16.3 metres from root intersection, and the support was positioned in 13.1 metres, see Figure 9.

Figure 9. Test set-up, test-series 1. The framed area is the down-wind surface of the same area as shown in Figure 7.

Both the applied load and the reaction force in the support were measured by use of force transducers.

During loading, data is recorded for the sensors and video cameras. The load is increased in steps, see Figure 10 and held for a short period of time to observe (via the video cameras) if damage evolves. When a significant amount of visible damage has developed, the wind turbine blade is unloaded and the blade is inspected by non-destructive techniques, which provide information of the internal (hidden) damage. Then, the blade can be subjected to a new load cycle.

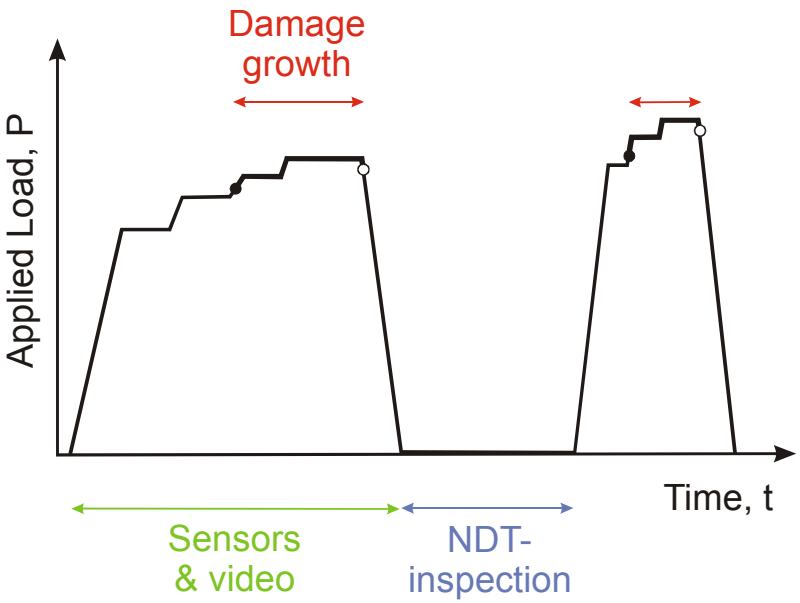

Figure 10. Principle of the loading history

4.4 Creating adhesive failure at trailing edge

The second damage was a removal of the glue in the joint in the trailing edge. An angular grinder was used to remove the glue. All glue in the trailing edge joint was removed over a distance of 0.40 meter. The artificial damage was made in a position 11 metres from the root intersection. Due to the slim size of the trailing edge the blade chord was shortened a little when the glue was removed, see Figure 11 and the trailing edge of up-wind and down-wind shells became very thin were the damage was made.

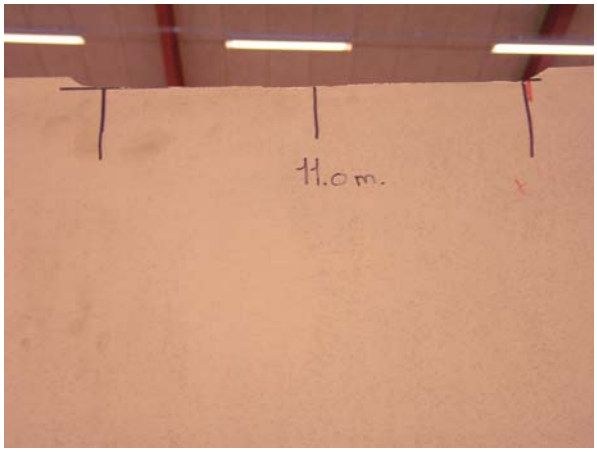

Figure 11. Down-wind surface

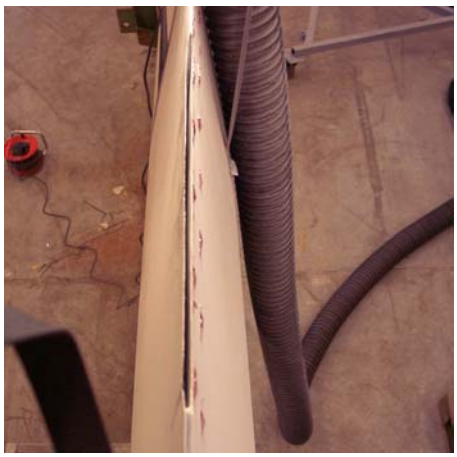

Figure 12. Damaged trailing edge

4.5 Mounting of optic micro bend displacement transducer

Optic fiber micro bend displacement transducer

The optic fiber micro bend displacement transducer is developed for this project. The development and the principles of the transducer are described in [Ref 4]. In short terms the principles are that a LED is used as light source, the light is send through a set of lenses into the optic fiber. The optic fiber is guided through a fiber-bending device. When the fiber is increasingly bended by the bending device the transmittance through the fiber is decreased. A laser detection unit (AM420) measures the light-transmittance through the fiber. The change in transmittance is related to the change in displacement between the two halves of the fiber bending device.

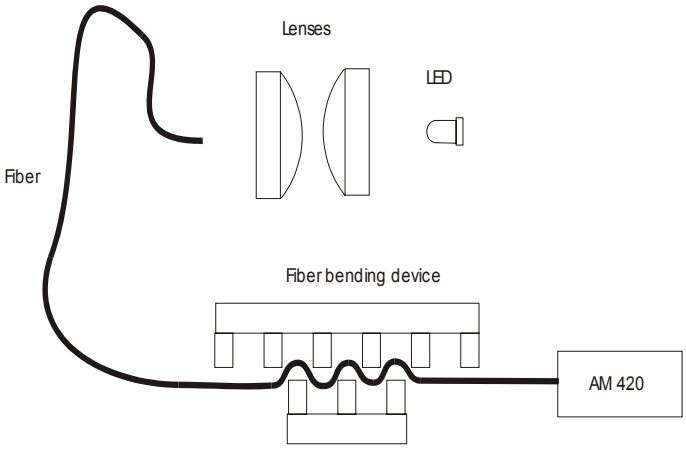

Figure 13. Sketch of micro bend displacement transducer set-up

Optimum transducer position

It was decided to test the transducer using two different methods for mounting. The aim was to mount the transducers in a way, which would be realistic in connection to future fabrication of the blades.

The simplest mounting is to mould-in the transducer in the adhesive layer, without any special attachment. The two shells are in the trailing edge glued together with a wedge shaped adhesive layer as shown in Figure 14.

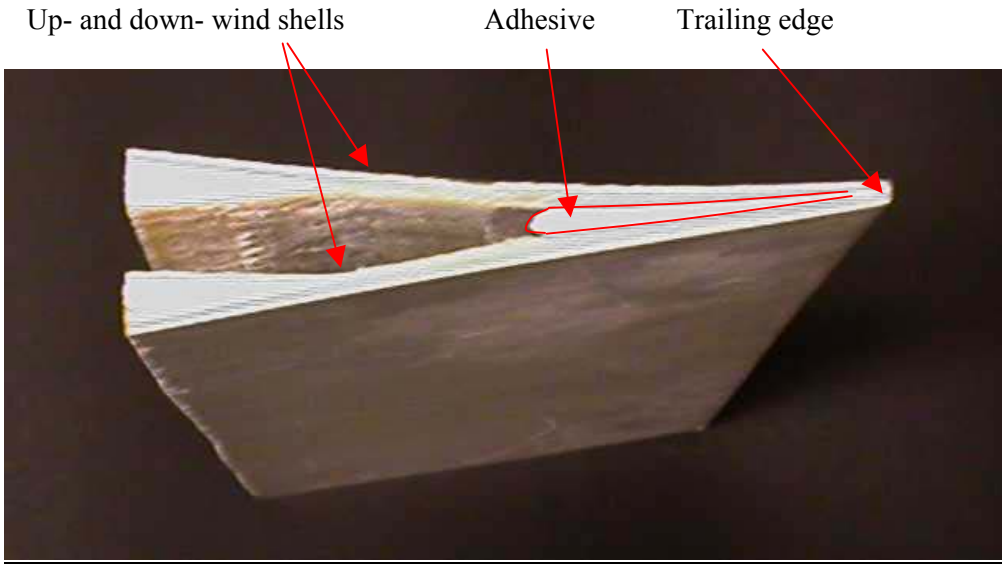

Figure 14. Cross section cut of trailing edge

The best position for the transducer is at the location where the distance between the to shells is equal to the thickness of the transducer. At this position the transducer must be expected to detect all cracks passing the transducer either in the adhesive layer or in the interface between the adhesive layer and the shells. If the transducer is located at a position where the distance between the shells is larger than the thickness of the transducer, the crack can pass in the layer of adhesive between the transducer and the shells, without causing any deformation detectable to the transducer. A crack in the interface layer is not anticipated to remove the contact between the shell and the corresponding transducer surface and should therefore also be detectable. The reason is that the surface of the transducer is freely moveable within perpendicular distance of about 0.2 mm, in contrast to the surrounding stiff adhesive. The 0.2 mm displacement corresponds to the maximum deformation of the fiber. Also transverse movement of the shells are expected to be absorbable by the transducer, so it will not loose its contact to the shells in connection with formation of minor cracks. The weakness of the simple mount is that the transducer will not detect cracks passing in the shells. To detect all cracks the transducer has to be connected to the outer surface of the shells. Another alternative is to create a connection to the outer surface of the shells.

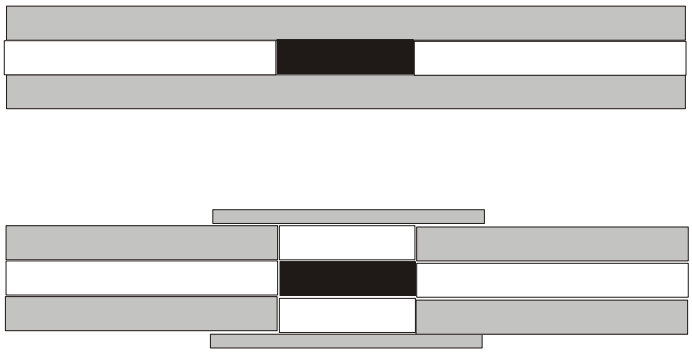

Figure 15. The two methods used for mounting of transducers. Above is the extremely simple mount where the transducer is moulded in between the shells. A hole is drilled though the blade in the second mounting method and the cylindrical cavity is closed with two plates of fibre composite material.

Mounting of transducer A

Using a silicone gun the notch was filled with adhesive to the level corresponding to the planned location of the transducer.

Because the trailing edge is wedge shaped (Figure 14) the sides of the notch closest to the trailing edge consist of glass-composite, but the sides in the bottom of the notch will consist of adhesive. The distance between the two shells is 5.5 mm (corresponding to the thickness of the transducer) in the transition-zone. This location was found by visual inspection of the sides, and in practice it was difficult visually to determine the material of the sides for several reasons. The visual inspection was done through a small gap and the notch was relatively deep. There was only a small difference between the visual appearance of the adhesive and the composite. Finally, the cut was not located in the centre of the adhesive layer, and the transition from fiber composite to pure adhesive did therefore not occur at the same depth of the two sides.

The transducer was smeared with adhesive, inserted into the notch and positioned in the transition zone.

The rest of the notch was filled with adhesive. It was a problem to fill the space behind the PTFE tubes guiding the optical fiber to the transducer. The X-ray pictures shows that there were cavities in the adhesive.

Mounting of transducer B

A 20 mm hole was drilled though the blade in the same distance from the edge, as transducer A was mounted. The rectangular transducer was positioned in the centre of the circular hole, between the two shells. Two minor pieces of polystyrene plate was inserted in the space between the to blade shells to fill up the hole completely in the region between the two shells. Copper grease was smear on each of the cylindrical sides in the two depressions, one of each side of the blade. The two cylindrical depressions were filled up with adhesive, and finally a square piece of fiber composite, coated with adhesive, were used to close the hole.

It was the intention that the two cylindrical plugs of adhesive on each side of the transducer bonded to the surface of the transducer and to the plate mounted on the surface of the shells, which again is fixated to the shells. The purpose of the copper grease was to prevent the adhesive to bond on the sides of the hole and the polystyrene plate pieces prevented the two plugs of adhesive to get in contact in the zones of the circular hole which is not occupied by the rectangular transducer. With this mounting method the transducer had god adhesion to the shells, and the deformation of the transducer was coupled to the movement of the outer surfaces of the shells, so that any crack, in the adhesive layer or in the fiber composite, could be detected.

4.6 Loading procedure and history

To make the damage propagate load was applied further towards the root than the damage. The load was applied downwards to create compression in the trailing edge. To cause this compression in the trailing edge a support was applied to the blade. The position of the load was 9.5 metres from root intersection, and the support was positioned in 13.1 metres, see Figure 16 and Figure 17.

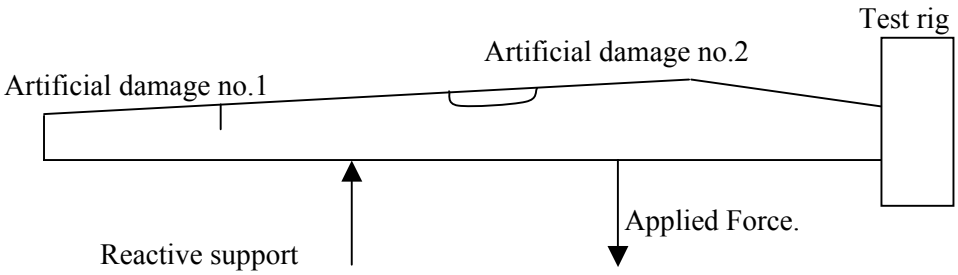

Figure 16. Principal sketch of test set-up and applied load and reactive support.

The position of the load was 16.3 metres from root intersection, and the support was positioned in 13.1 metres.

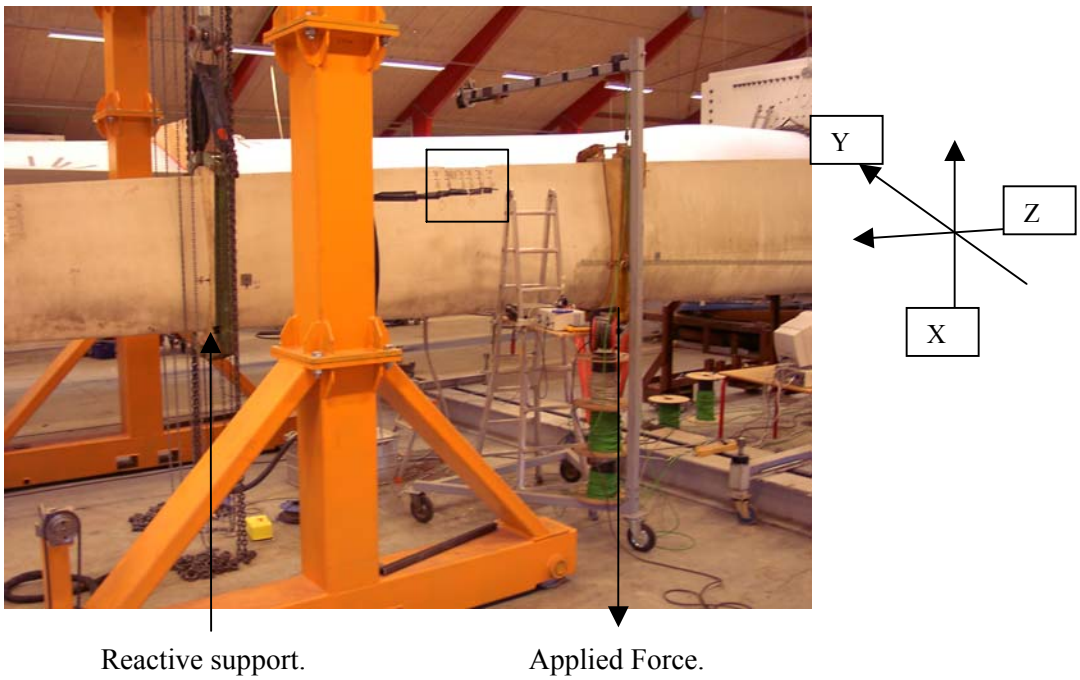

Figure 17. Test set-up for damage no. 2. The framed area is the down-wind surface of the same area as shown in Figure 18.

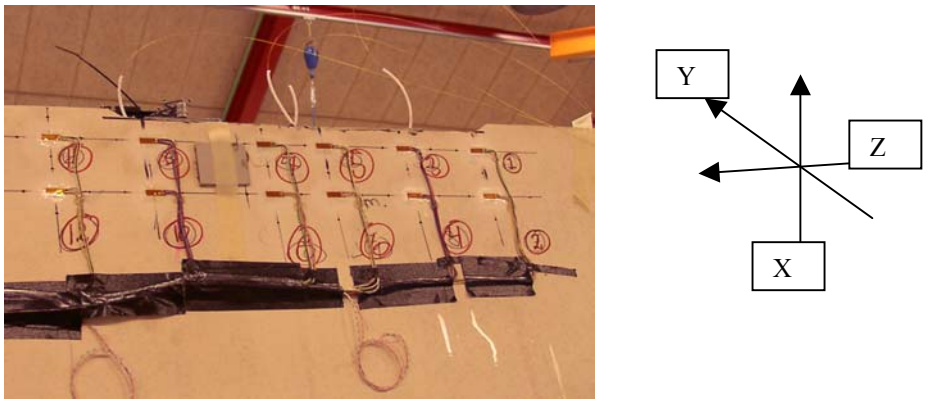

Figure 18. Down-wind surface of blade, damage no. 2. Tip-end direction to the left.

5 Results for damage in laminate

5.1 Overview

The test of the failure in the laminate was carried out in different steps as listed in Table 3.

Table 3. Name and time for the individual tests

	Test-no.	**Time of start, videotape**	**Time of start**
Damage no. 1	WING001	0h 05m - 00h 11min	15/1/02 kl. 16.26
	WING002 (cancelled)	0h 13m	
	WING003	0h 23m 30s	15/1/02 kl. 18.06
	WING004	0h 31m 46s	16/1/02 kl. 08.35
	WING005	0h 51m 03s	16/1/02 kl. 10.15
	WING006	1h 21m 00s	16/1/02 kl. 12.11
	WING007 (cancelled)	1h 49m 05s	
	WING008	1h 57m 01 s	16/1/02 kl. 14.56

The damage propagated in a rather stable manner; a higher and higher load was required to cause the extension of the damage front into the blade.

As the load was increased stepwise, it was possible to grow the cracks in quite small steps, as indicated in Table 4.

Table 4. Test-name and damage propagation measured by visual inspection of damage.

test #	**UPWIND (pressure side) SG1-5 & SG11-15**			**DOWNWIND (suction side) SG6-10 & SG16-20**		
	crack length at start of test mm	**growth during test mm**	crack length at stop of test mm	crack length at start of test mm	**growth during test mm**	crack length at stop of test mm
WING001	0	**0**	0	0	**0**	
WING002						
WING003	0	**5**	5	0	**4**	4
WING004	5	**14**	19	4	**3**	7
WING005	19	**81**	100	7	**25**	32
WING006	100	**14**	114	32	**88**	120
WING007	114	**0**	114	120	**0**	120
WING008	114	**11**	125	120	**30**	150

As part of the post-mortem, sections containing the damage were cut from the upwind and downwind laminates of the blade. Figure 19 and Figure 20 illustrate the ultimate extension of the damage in the upwind laminate, as found on the external and internal laminate surfaces, respectively.

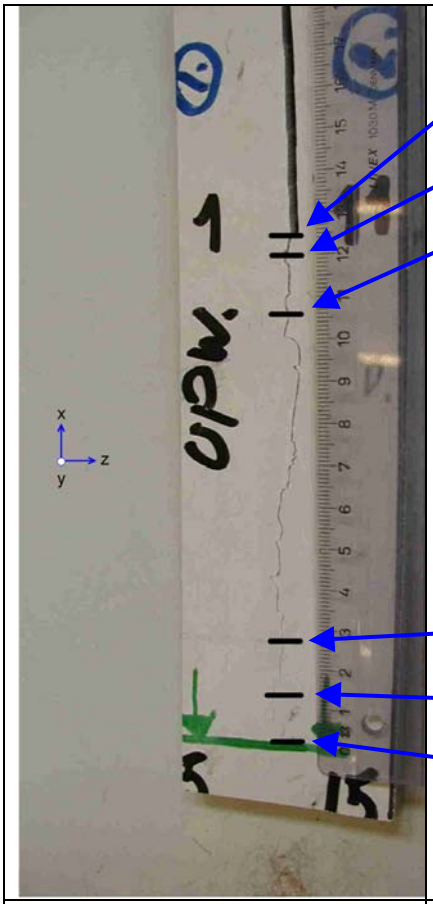

Figure 19. Crack-like damage in the external surface of the upwind laminate.

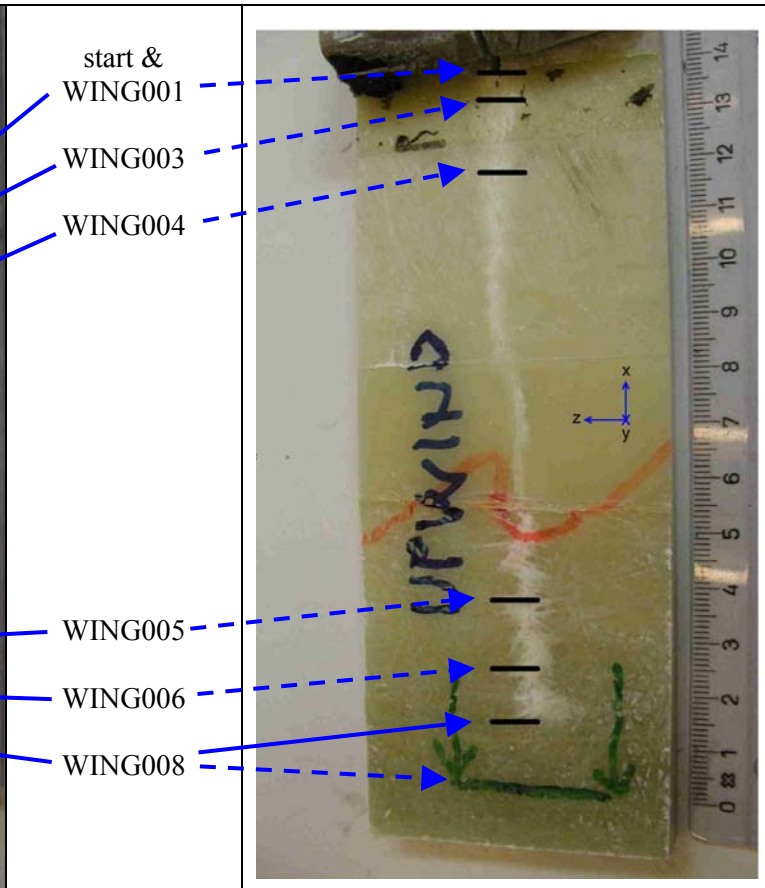

Figure 20. Diffuse damage in the internal surface of the upwind laminat (dashed arrows indicate estimated damage front positions).

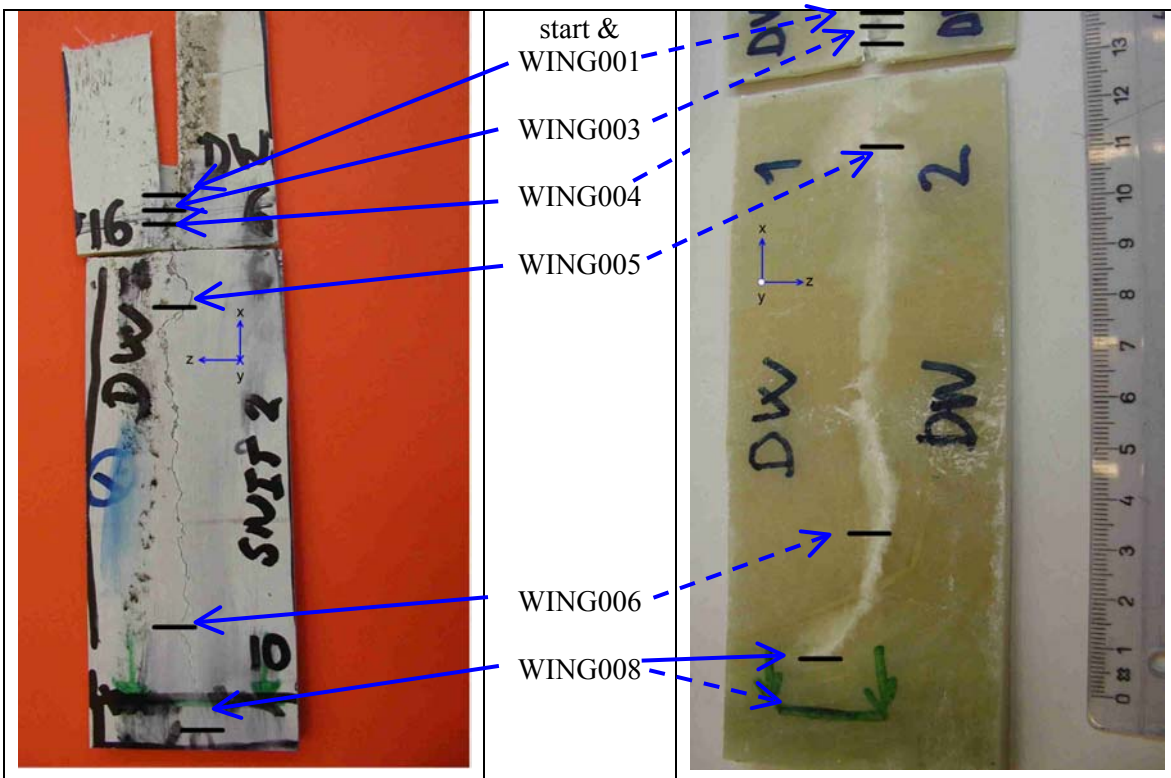

Figure 21. Crack-like damage in the external surface of the downwind laminate.

Figure 22. Diffuse damage in the internal surface of the downwind laminate (dashed arrows indicate estimated damage front positions).

The damage extending from the pre-cut notch appears as a hair-line, crack-like damage on the gel-coated external surface, Figure 19. The same damage, as seen on the internal un-coated surface, is of a more diffuse nature, displaying a greater width (between 3 mm and 12 mm) with signs of delamination and bifurcation, Figure 20. In addition, the ultimate damage extension is less on the internal surface, as compared to the external surface. The damage is not like a crack, since the two faces of the damage are linked by fibres bridging the faces.

In Figure 19 and Figure 20, bars set perpendicular to the direction of damage extension illustrate the extent of damage development following the loading steps WING001 through WING008, as recorded in Table 4. It is seen that loading step WING005 resulted in the largest, singular increase in extension. During loading steps WING003 and WING004 extensive delamination and crack bifurcation was experienced, Figure 20.
Corresponding information regarding the damage development in the downwind laminate is given in Figure 21 and Figure 22. The damage seen here is generally of the same nature as that in the upwind laminate. But the amount of delamination and deviation appears to be more extensive - especially so during and at the end of loading step WING005 (25 mm) - and the damage deviation during the final loading step is larger, Figure 22. In this laminate, the largest extension was obtained in loading step WING006. It should be noted, that the laminate thickness increases away from the trailing edge (in the negative X-direction). This, together with the fact that crack bridging occurred in the entire damage zone may explain why a higher and higher load was required to propagate the damage front deeper and deeper into the blade.

The result (the propagation in crack length) of each of the tests for damage no.1 is shown in Table 4. The presentation of results is limited to the tests called WING 001, WING 003, WING 004, WING 005, WING 006 and WING 008. These tests are described in the following paragraphs.

5.2 Strain gauges results

Hardware details

Data acquisition system:
HP 75000 Strain gauge system
Daqwin-programme, LabView software
CEA-06-500UW-350 Strain Gauges, Measurements Group Inc
HBM Loadcells and ASM displacement transducers.

General observations on the SG measurements

To measure the strain distribution in the area of the damage, 20 strain gauges were mounted on the blade in the area of damage 1; see Figure 23 and Figure 24. The exact position of the gauges are shown in Figure 25.

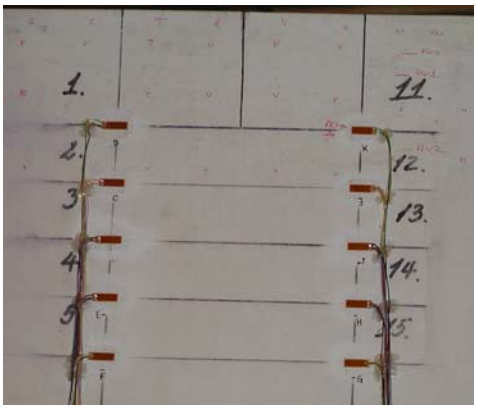

Figure 23. SG-pos. damage 1 Up-wind

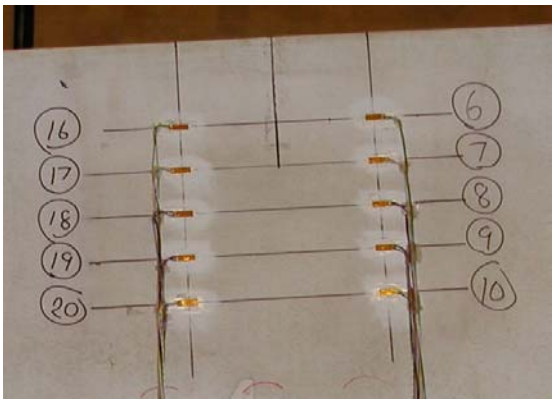

Figure 24. SG-pos. damage 1 Down-wind

On the two pictures the tip-end of the blade is towards the middle of the page.

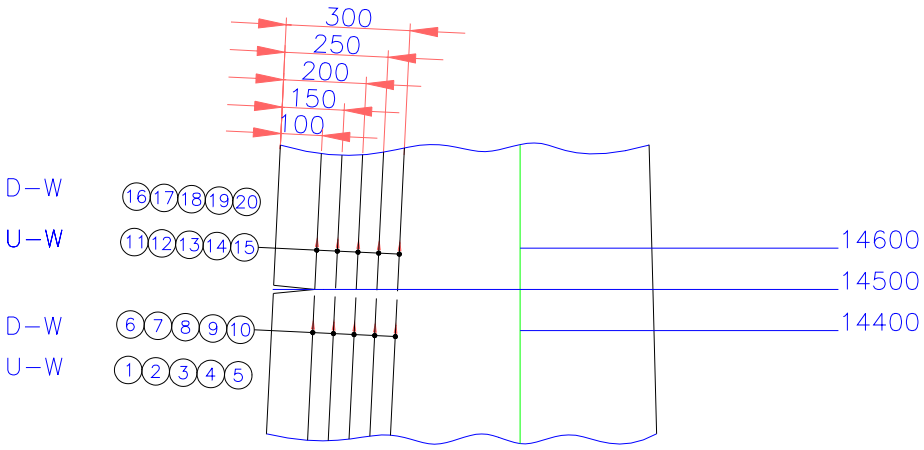

Figure 25. SG-positions damage 1

The artificial damage no. 1 had a length of 98 mm i.e. the damage ended in the line between the strain gauges closest to the trailing edge (SG-no. 1, 6, 11, 16).

Results WING004 through WING006

The sampled strains as function of time, from test-series WING001 to WING008, are shown in Figure 26. Each of the peaks in the graphs represents the max. strain level for each load series, see numbering of load series in paragraph 3.3. Load series “WING 007” is not presented in the graphs because it was cancelled.

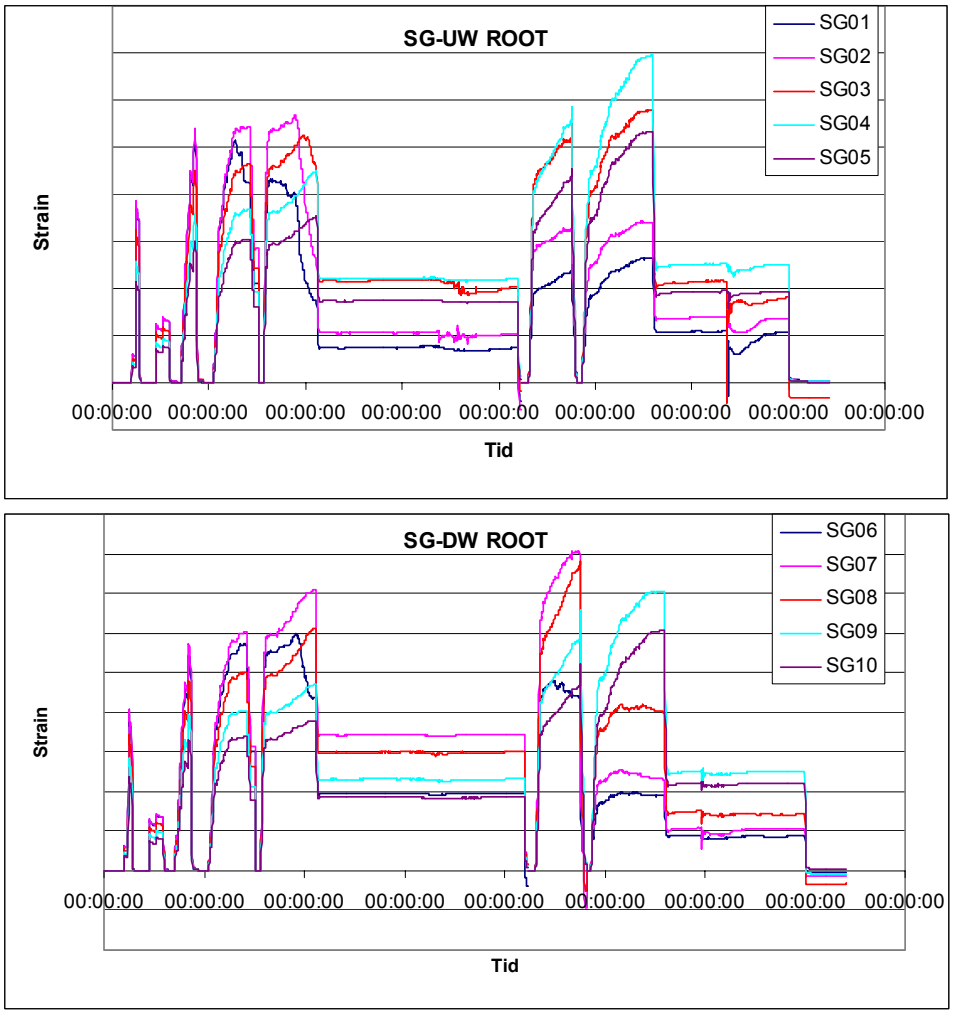

Figure 26. SG-measurements from test WING001 – WING008, Damage no. 1.

As the load was applied to the blade a linear related increase in strain level was measured on all the strain gauges. The relation in strain level between the strain gauges was also linear in correspondence to the distance from the neutral line of the blade, except for the 4 strain gauges (SG-no. 1, 6, 11, 16) in the line of the tip of the damage, which showed a lower strain level. The linearity ruled for tests “WING001 to “WING003”. During test “WING004” the strain level for the gauges (SG-no. 1, 6, 11, 16) nearest the trailing edge decreased while the next gauges (SG-no. 2, 7, 12, 17) were increasing in strain level, this change is indicated in the red arrows in Figure 26. The change in strain level was highest on the up-wind side of the blade; this corresponds with the growth of the damage during this test. This change in strain level between the strain gauges corresponded to the propagation in the crack length.

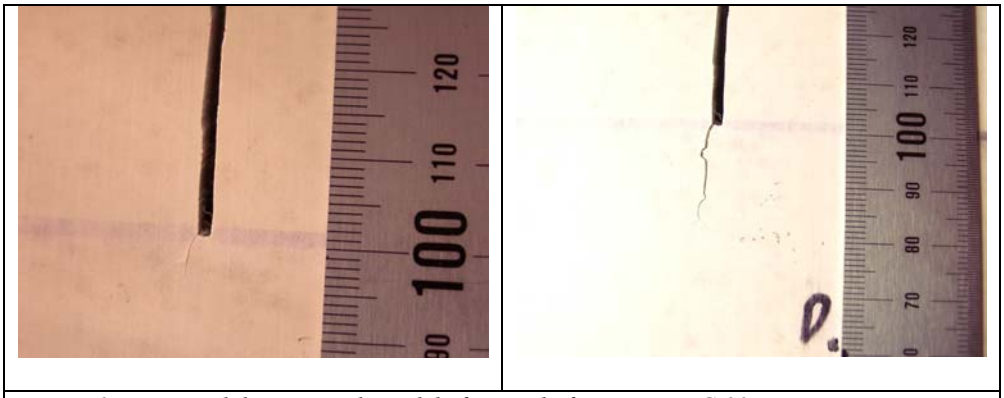

Figure 27. Up-wind damage and crack before and after test WING 004.

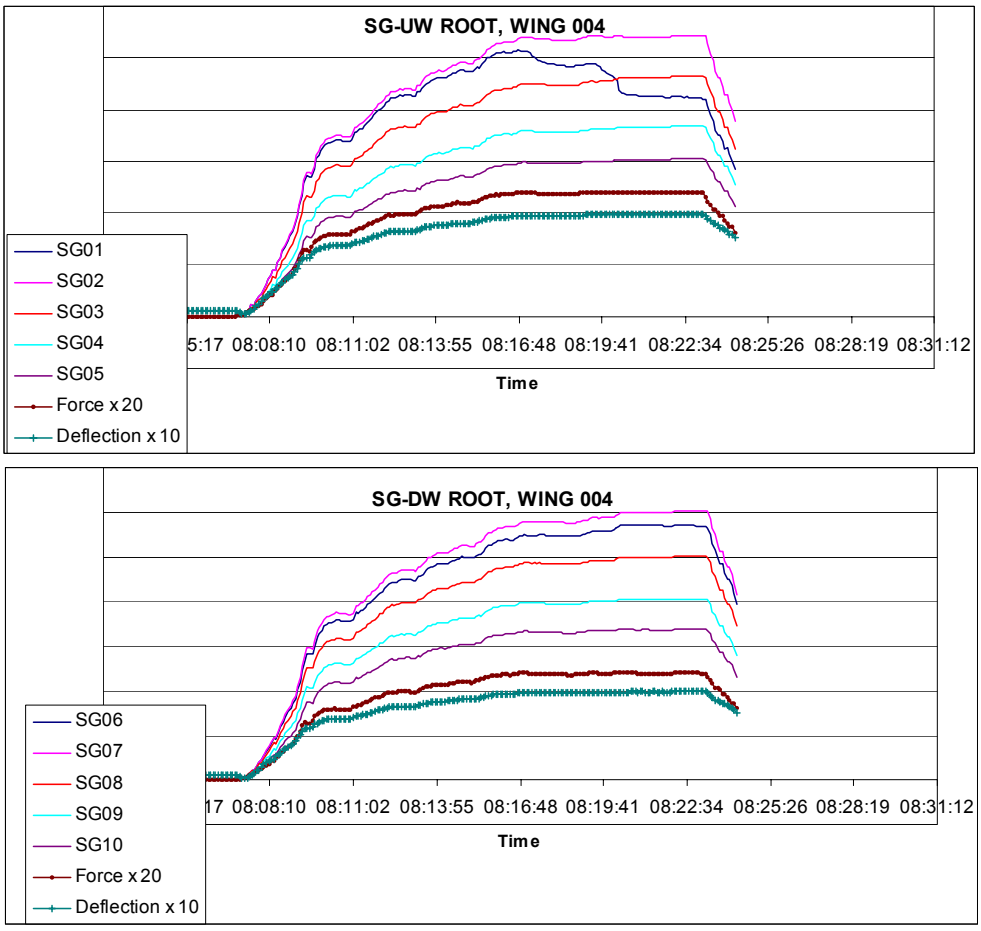

Figure 28. Measured strain, force and deflection as a function of time during "WING004"

For test "WING 005" and "WING 006" similar changes in strain level was seen in correspondence to the propagation in the damage.

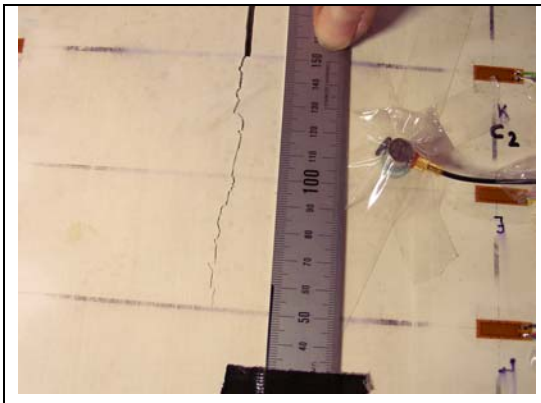

Figure 29. Up-wind damage after WING005 (note AE sensor , right side)

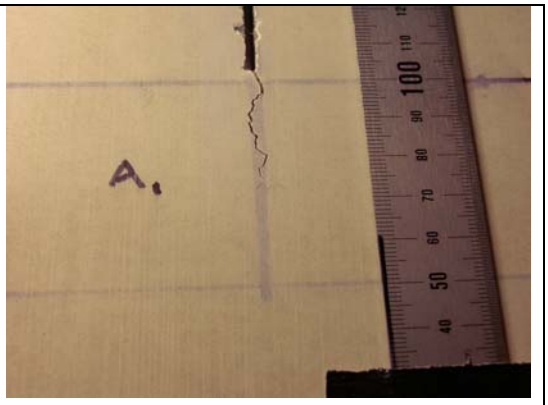

Figure 30. Down-wind damage after WING005

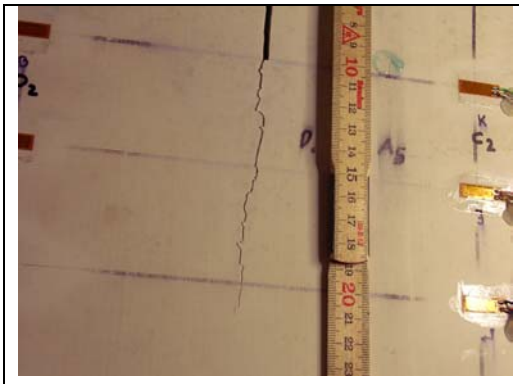

Figure 31. Up-wind damage after WING006

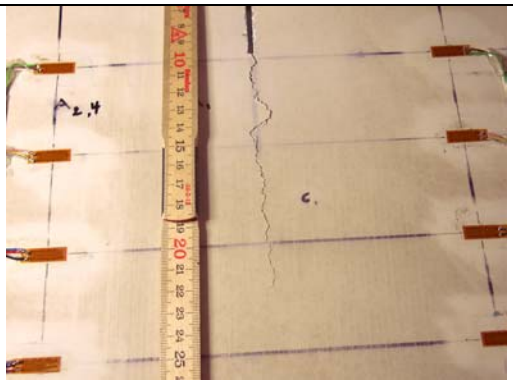

Figure 32. Down-wind damage after WING006

The major difference between WING005 and WING006 is the duration of the crack propagation. During WING 005 the crack propagated over a little less than 10 minutes, and during WING 006 the same size of damage propagation happened within the same minute. This is seen as a very steep change/decrease in the strain level for strain gauge no. 08 at the end of WING 006. Note, that the decrease in strain level appears prior to the unloading/decrease in load level.

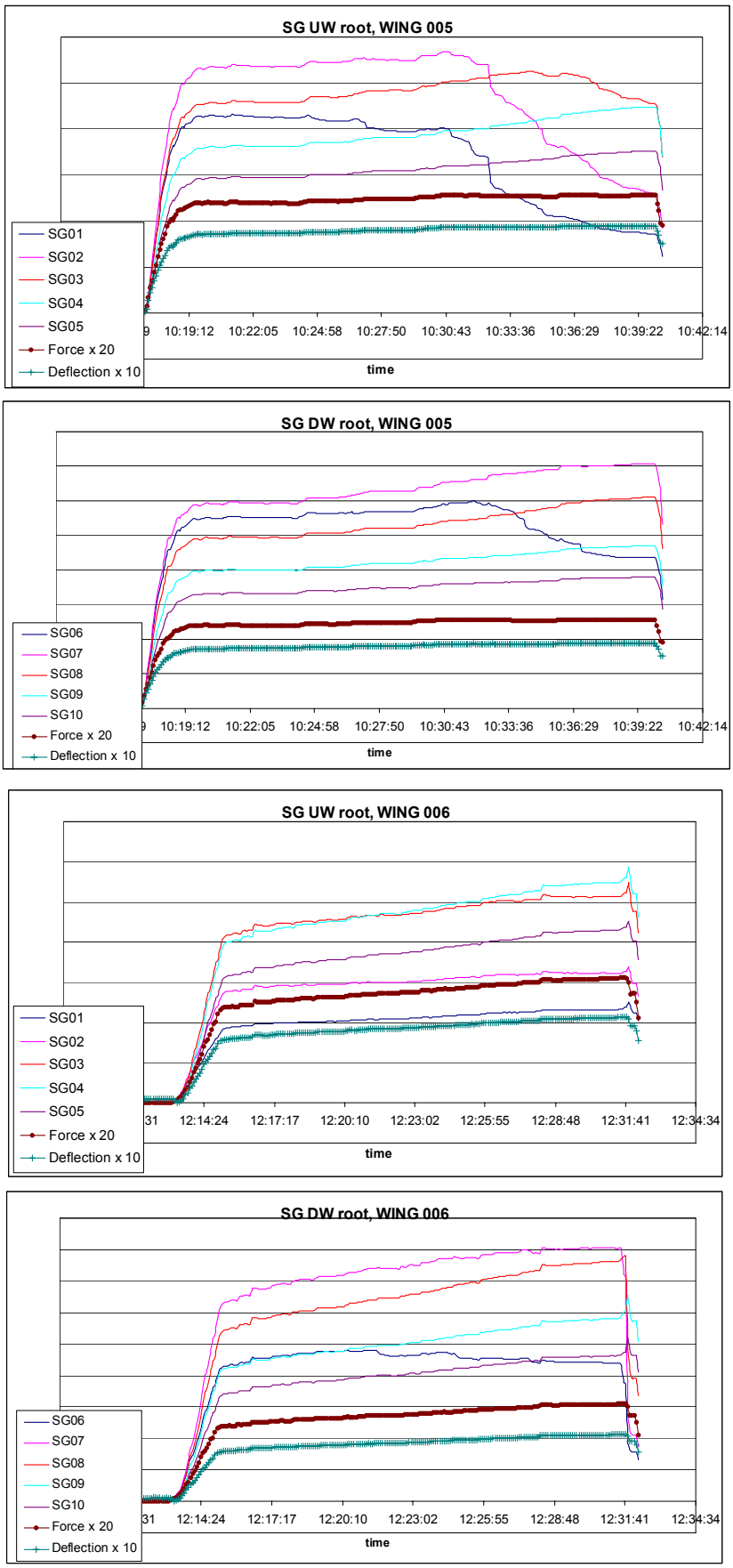

Figure 33. Strain measurements during WING 005 and WING 006

5.3 Acoustic emission results

Hardware details

Two independent Acoustic emission (AE) systems were used during the static blade tests held at Sparkær.

System one
Physical Acoustic SPARTAN AT
Two channel system
PAC U80-220 micro80 piezoelectric sensors
Zonal or linear source locator function
Relevant system settings (Gain 20dB, THS 45dB, PDT 50μs, HDT 200μs, HLT 300μs)
Waveform characteristics recorded for each hit (Amplitude, Energy, Counts, Rise Time, Average Hz)

System two
Labview controlled waveform recorder
Two channel system
PAC U80-220 micro80 piezoelectric sensors
pre-triggered waveform display

The micro80 piezoelectric sensors used were attached directly to the test structure using adhesive tape. No surface preparation was necessary. An ultrasonic couplant gel (Krautkrämer Hürth ZG-F) was used to ensure good contact with the test structure. The AE sensors were routinely removed between each test loading to allow NDT scanning of the damaged area. Sensor function was checked by performing a pencil leadbreak test.

General observations on the AE sensing

Both AE systems were used during all the testing carried out at Sparkær. The following general observations were made.

Mechanical testing of large structures poses risks to people and equipment that are in close proximity. For this reason all those involved in the testing remain at a safe distance while the test is under load. This remoteness from the structure can make controlling the test more challenging, as was the case at Sparkær, where a high load was applied to a 19m long structure that resulted in only a small area of damage. The problem requires the use of video cameras that the controller can use to check signs of damage progression. The audible signal generated by the SPARTAN AT system provided a useful non-visual feedback for the test controller as the load was slowly increased in a stepwise manner.

The first acoustic hits detected by the system are believed to have resulted from microdamage such as matrix cracking and fibre breaking, since no macrodamage could be found at this stage by any other means. These hits indicated when the load was approaching the point where crack growth becomes possible and care must be taken in applying further load. At this stage no change in the video images could be observed. A definite increase in hit numbers and intensities indicated when macrodamage (such as crack growth and delamination) were beginning to take place. This clear distinction between the audible signals returned by the system allowed the test operator greater confidence in controlling

the progress of the damage within the structure. The growth of the damage area was confirmed by visual, ultrasonic and X-ray inspection between loadings.

Linear and Zonal source locator functions in the SPARTAN system were utilised during the testing and gave good indications that they reflect the position of damage directly observed during the NDT inspections between loadings.

Two classes of damage waveform were displayed on the Labview AE system during testing, and examples of these are shown. The damage waveforms were identified as either microdamage (from matrix cracking and fibre snapping) or macrodamage (from laminate cracking and adhesive splitting). The waveforms were recorded by the Labview system when the voltage reading on the transducer spiked above the user defined "trigger level". This trigger point is always at 250μs in these traces.

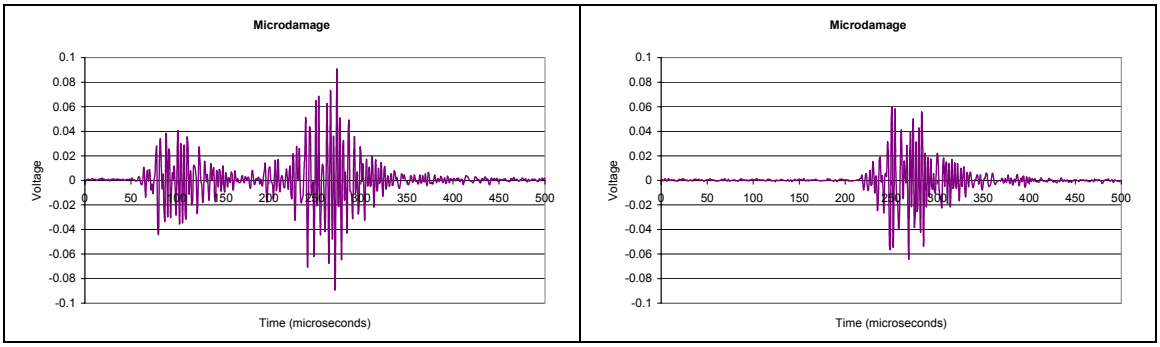

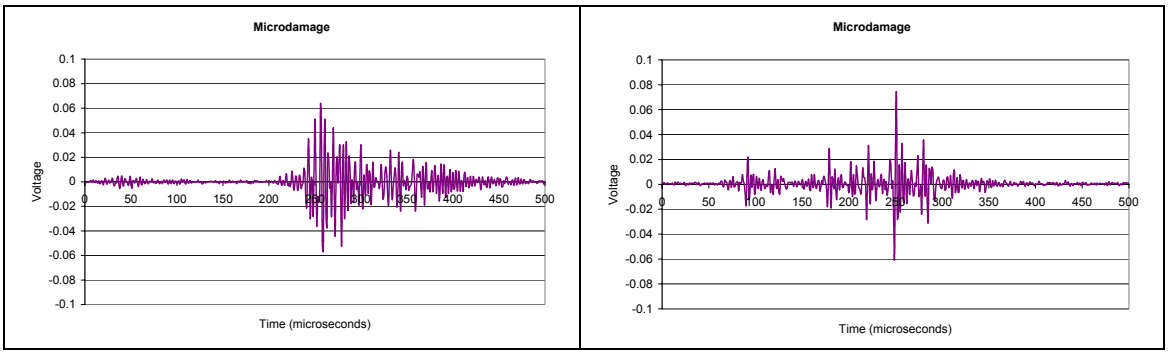

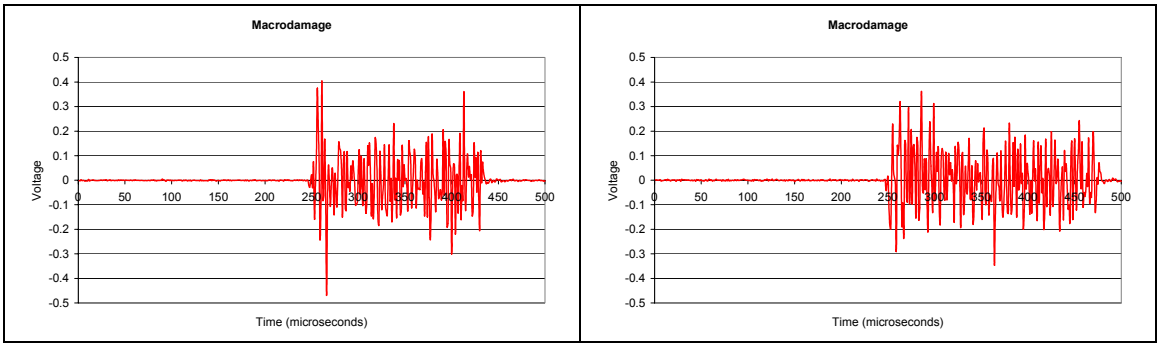

The microdamage waveforms are generally of a lower amplitude and shorter duration than those caused by macrodamage. This is due to the fact that the macrodamage waveforms are essentially due to a friction source event whereas the microdamage waveforms are caused by a discreet point event such as a matrix crack or fibre snap. The form of the microdamage waveforms is also sig-

nificantly different, being a more "classical" AE response where the signal oscillates up to a maximum and then dies down in the same way. Also significant in the microdamage signal is the presence (or absence) of smaller pre-signals in the recorded waveform; these result from faster moving waves propagating from the same source event. Correct interpretation of the pre-trigger signal can give information about the distance and even the orientation of the source relative to the transducer.

It proved possible to place "early warning" sensors to help control the damage created in the structure by the test loading. Both sets of static test on the blade were designed to create a very specific damage type, any "alternative" damage was unwanted. Therefore, in those cases where there was judged to be a risk of damage occurring at a point on the blade where it was not wanted a sensor from the Labview system was positioned there. This could be at the "clamped" end of an adhesive crack or at the loading yokes. During testing, any activity from this specific sensor warned the test controller that there was unwanted damage occurring, the test could then be aborted and corrections made.

Source locator function

Four sensor placement strategies were used with the SPARTAN AT system during test series 1.

Near/Far Zonal location
Here one sensor (channel 1) was placed directly adjacent to the initiator crack and the other was placed at a point on the structure far from any anticipated sources. This short test (WING001) lasted only 13 minutes and produced no actual crack growth; in fact it produced no damage detectable with either visual inspection or ultrasonic and X-ray NDT. However the AE sensor placed adjacent to the crack initiator recorded 1949 AE hits with a total energy content of 24027, (Figure 34), while the sensor (channel 2) placed away from the crack initiator recorded no activity.

This simple test demonstrates the potential of the sensitive AE transducers to monitor events at levels below the severity necessary to cause damage detectable by traditional inspection. It also shows that the test has been successfully designed to preferentially promote damage in the desired location.

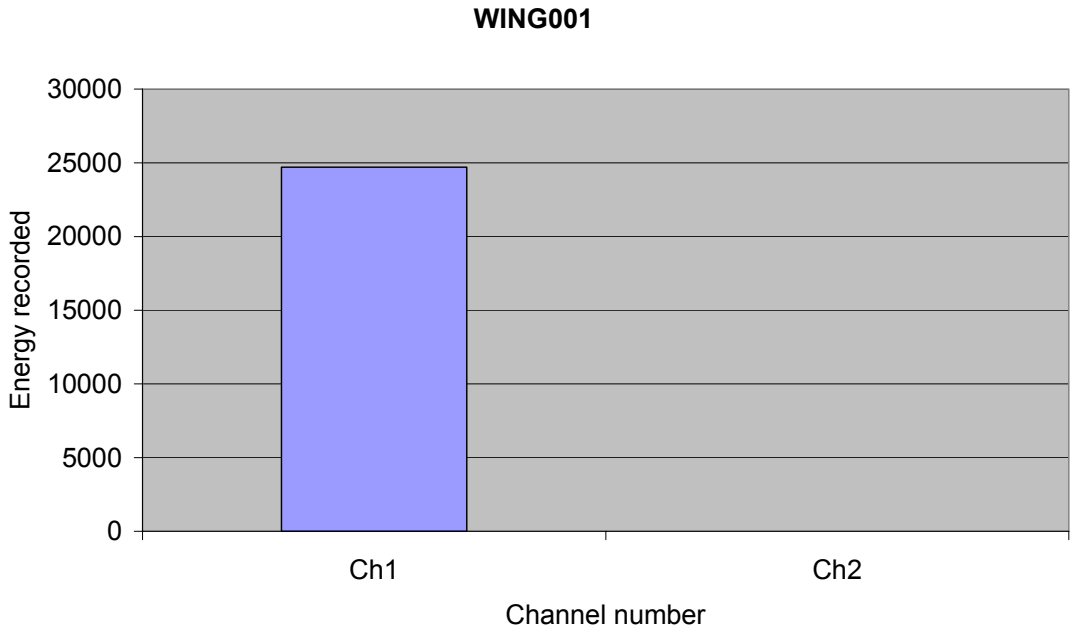

Figure 34. Zonal location for WING001

Tip/Root Linear location

In these tests (Figure 35 and Figure 36) the sensors were placed (300mm apart) on either side of the vertical crack. One sensor was positioned 100mm towards the blade tip side of the crack and the second sensor was placed 200mm away on the root side. For each hit detected by both sensors the system uses a time of flight calculation to determine the source of that hit. Thus a distribution of the AE activity along the horizon between the two sensors is created.

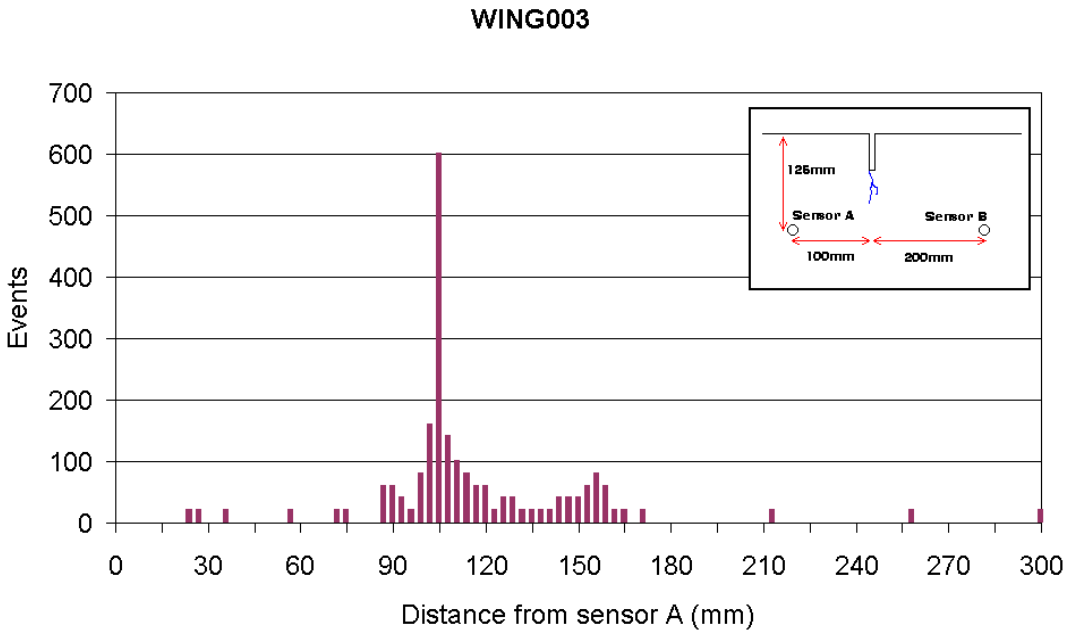

Figure 35. Linear location of AE events for WING003 at end of test

This graph clearly shows a high concentration of AE "events" between the two sensors at precisely the position of the crack.

This test was repeated in WING004.

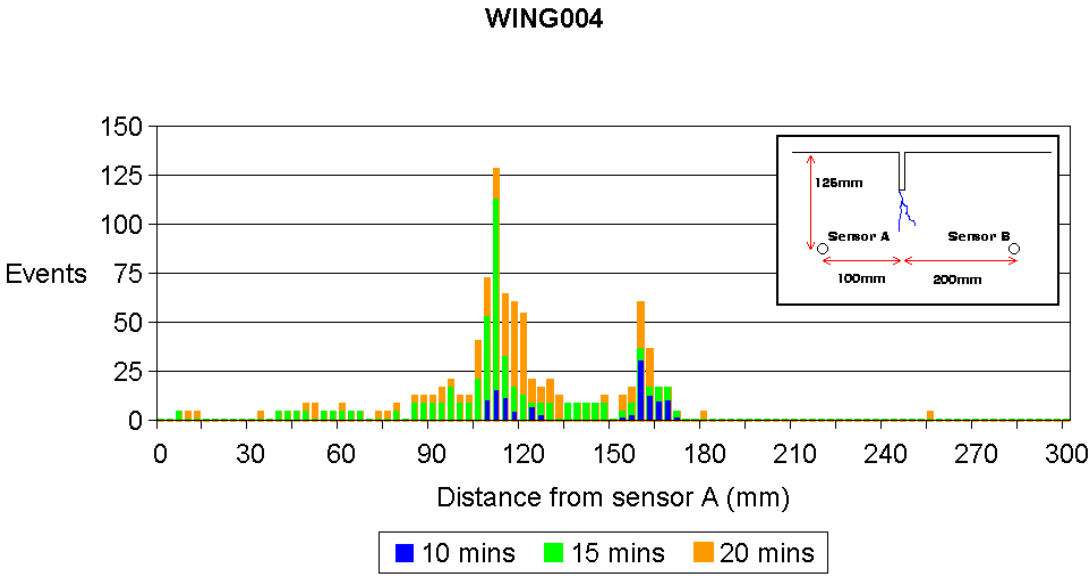

Figure 36. Linear location of AE events over time in WING004

It is interesting to note in Figure 36 that a second peak has developed to the root side of the main source corresponding to the crack tip. Indeed this secondary source is the more active at the beginning of the test. The presence of this secondary source is also discernible, although not so strongly, in Figure 35. Photographs subsequently taken of the damage shows crack branching on the downwind side that is in agreement with a secondary source.

Lead/Trail Linear location

In these tests the sensors were set up in a linear location array parallel to the direction of the crack. In WING005 both sensors are below the crack tip and anticipate the movement of the crack into the area monitored by them, see Figure 37.

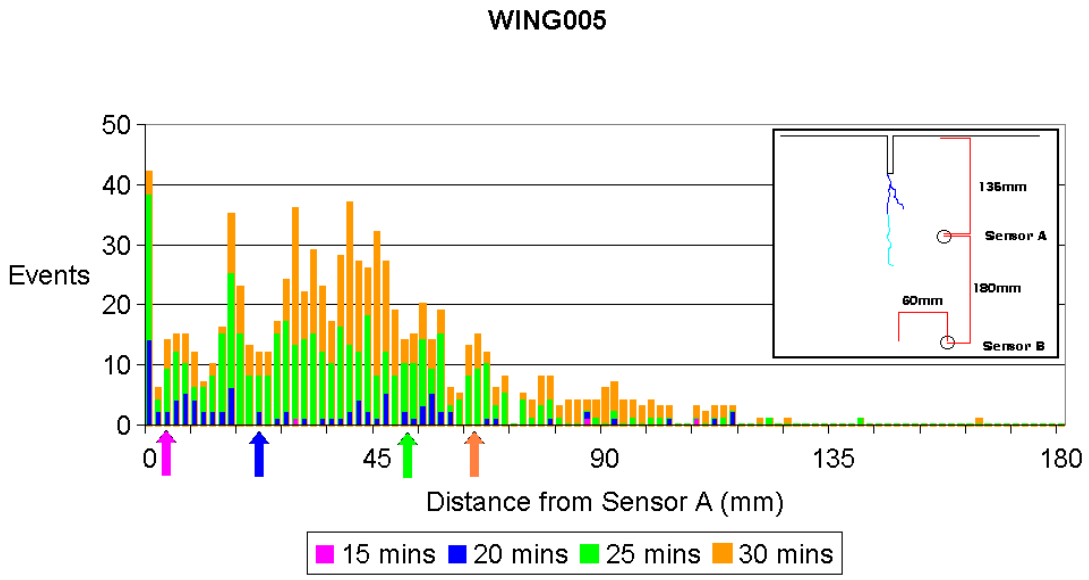

Figure 37. Linear location of AE events over time in WING005 (arrows indicate crack tip positions taken from video images)

During this test the crack advanced 81mm on the upwind side, where the AE sensors were positioned. During the early part of this test the crack front was above the sensor array, and as the graph shows very few hits were recorded by the location array during this time. However, as the crack moved downwards into the area monitored by the sensors (from the left in this graph) the AE events become more frequent and track to the right as the crack advances. The general location of the crack front at four time intervals and the graph display at that time are indicated by colour coding.

The test was repeated in WING006, but this time the sensors were positioned so that the crack tip began within the monitored area, some 75mm from the sensor nearest the trailing edge. Figure 38 shows a broad source of AE events at the crack tip, it should be noted that the crack advanced only 14mm during this test.

It can be seen that the point resolution for the crack tip in the "vertical" direction (trailing to leading edge) for the locator shown in WING005 + 006 is less clear than that observed in the "horizontal" direction (tip to root) shown in WING003 + 004. This is expected due to the nature of the damage type, which is a linear crack travelling in one plane along a chord of the blade.

In WING003 + 004 the crack is generally travelling down one point on the plane between the sensors. In WING005 + 006 the crack is travelling along the plane between the sensors and a distribution of hits along the length of the crack line is generated.

It is clear from Figure 37 and Figure 38 that the AE events are not only being generated at the cracktip, this is agreement with visual observations. In a cracking composite material (unlike metals) the crack wake also contains multiple sources of damage such as fibre pullout. There is therefore *a long damage zone*

associated with a crack in fibreglass reinforced plastics, not just damage at the tip.

At this point it would have been ideal to create a three or four channel planer location array. However, hardware restrictions on the SPARTAN system being used prevented this. A planer array of this kind would effectively combine the event activity distributions similar to the types found in WING003 (the x-axis coordinates) and WING005 (the y-axis coordinates) to produce a 2D view of AE event activity around the crack tip. In effect a detailed "map" of the location and activity of a repeating stress wave emission source.

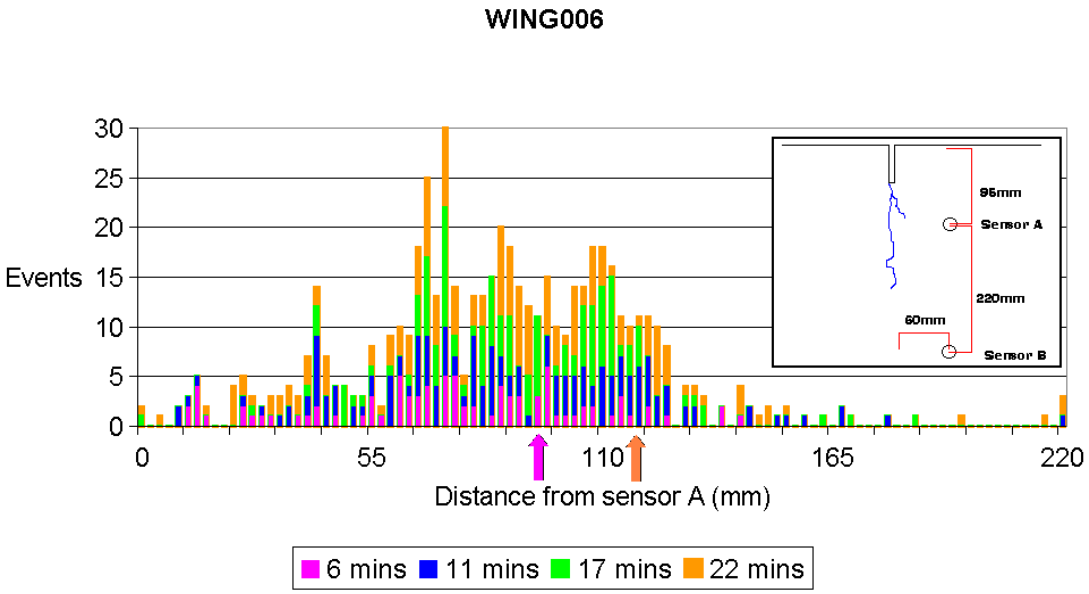

Figure 38. Linear location of AE events over time in WING006

Upwind/Downwind Zonal location

In this test one sensor was placed on either side of the blade (Upwind and Downwind) adjacent to the crack tip on that side (Figure 39). A zonal location type was utilised where every AE event detected is registered to either one sensor or the other, depending on which sensor detects it first.

Video images during the test confirmed that the crack advance on each side was not symmetrical. The Upwind (pressure side) crack advanced 11mm during WING008 and the Downwind (suction side) crack advanced 30mm. A rough indication of the crack growth visible on either side of the blade is shown in Figure 39. These readings are only estimates based on viewing of the surface recorded on the test video.

In general the crack growth was at a steady rate, however there are occassions when the crack was seen to grow a few milimetres comparatively quickly. These instances have been higlighted on the graph with colour coded arrows.

Figure 40 shows the combined energy received by the two AE sensors during the course of WING008. The crack growth indicators established in Figure 39 are shown again here. As might be expected the periods of highest combined energy generally correspond to the periods of crack advance established in Figure 39.

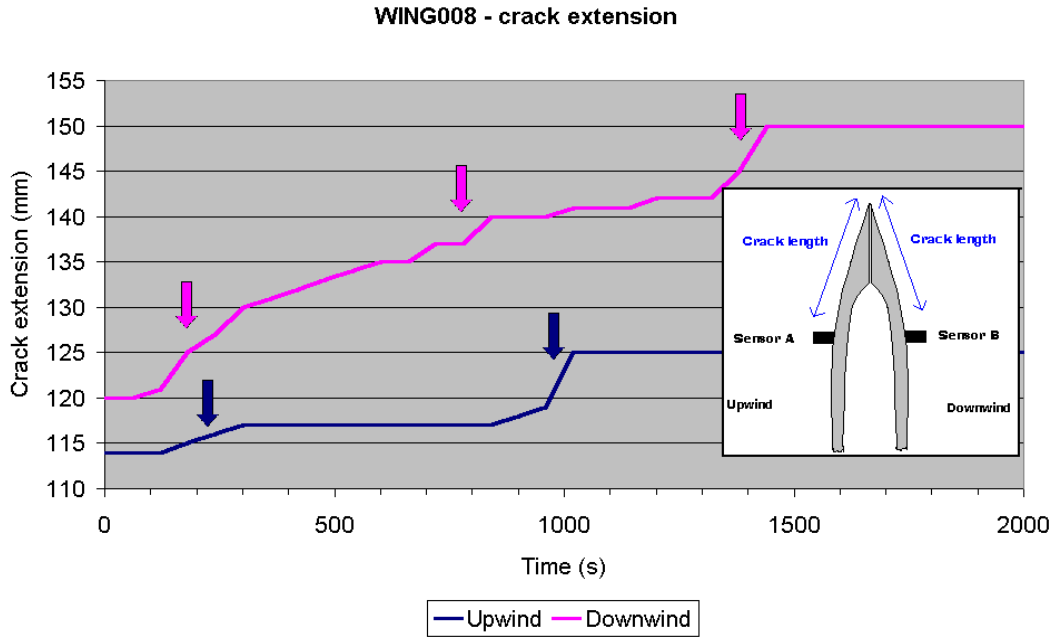

Figure 39. Crack extension on either face over time during WING008 test

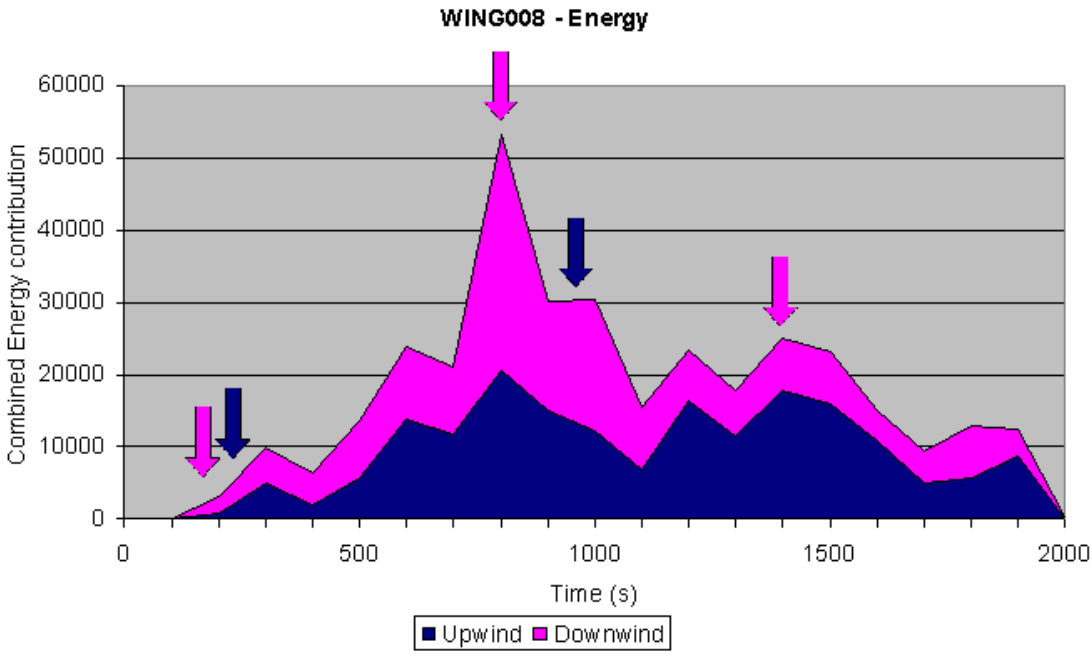

Figure 40. Accumulated energy detected from both sensors during test WING008

Summary of AE measurements taken during blade test

- Surface mounted AE sensors can be used to detect damage events occurring within the test structure.
- AE signals have been detected at sub-critical load levels, that is prior to damage visible with visual, ultrasonic or X-ray NDT.
- Zonal and/or Linear (time-of-flight) localisation has been demonstrated.
- Different types of AE waveform signals have been recognised.

5.4 Ultra sonic inspection

Hard ware details

P-Scan Equipment; PSP-3 Ultrasonic box with amplifier and data acquisition system, PC-PROG software, AWS-6 Manipulator and vacuum-rail for mounting on blade.

Methodology

In the production of advanced fibre-reinforced composites, ultrasonic inspection techniques plays today an important role in the quality control, due to the fact that this method effectively detects most of the relevant defects such as:

- Delaminations
- Missing adhesion and missing adhesive between bonded structures
- Dry spots, voids and porosity in laminates
- Irregular lay-up (thickness or scattering variations)
- Foreign bodies, (such as peel-ply)

Since the above mentioned defects are oriented at right angles to an ultrasonic wave propagation at normal incident into a laminate, they are ideally aligned for detection by ultrasound. Ultrasound is widely used on composite structures in the field as well as in the laboratory.

In this case, ultrasound inspection of the crack development (damage no.1) has been performed by means of a flexible automated ultrasonic scanning system developed by FORCE Technology (P-scan). This equipment consists of a vacuum mounted scanner unit, which moves the ultrasound transducer systematically covering the surface to be inspected. During the scanning echo amplitudes are collected together with the transducer position and stored digitally. The results can be evaluated on-line during and after scanning on a portable PC.

Figure 41. The flexible scanner mounted by means of vacuum on the wind turbine blade (damage no. 1).

After each test ultra sonic inspections (US-I) were made of the damage to have an estimate of damage size. To have a basis for the ultra-sonic determination of the damage propagation two ultra-sonic tests were made on the blade before the tests of the blade were carried out. The first US-I was made when the undamaged blade was mounted on the test rig and the second US-I was made after the artificial damage was made on the blade.

The initial inspection of the blade was carried out in the area from 11600 mm from root intersection and till 14000 mm. The inspected area was separated in sections of 400 mm in longitudinal direction and all sections had a size of 320 mm in angular direction measured from trailing edge.

The results from the ultrasonic inspections are further described in [Ref. 6].

Test	**Comments to scanning-results.**
	Reference examination. OK.
	Examination of torn out fibres after grinding of notch. OK.
WING 001	No visible propagation in damage subsequent to unloading.
WING 003	No visible propagation in damage subsequent to unloading.
WING 004	No visible propagation in damage subsequent to unloading.
WING 005	Increased damping in the area app. 65 mm from notch.
WING 006	Further damage propagation, app. 45 mm.
WING 008	Further damage propagation, app. 15 mm.

Figure 42. Table showing ultra sonic results of inspection of up-wind side of blade

Test	**Comments to scanning-results.**
	Reference examination. OK.
	Examination of torn out fibres after grinding of notch. OK.
WING 001	No visible propagation in damage subsequent to unloading.
WING 003	No visible propagation in damage subsequent to unloading.
WING 004	No visible propagation in damage subsequent to unloading.
WING 005	Increased damping in the area app. 25 mm from notch.
WING 006	Further damage propagation, app. 85 mm.
WING 008	Further damage propagation, app. 15 mm.

Figure 43. Table showing ultra sonic results of inspection of down-wind side of blade

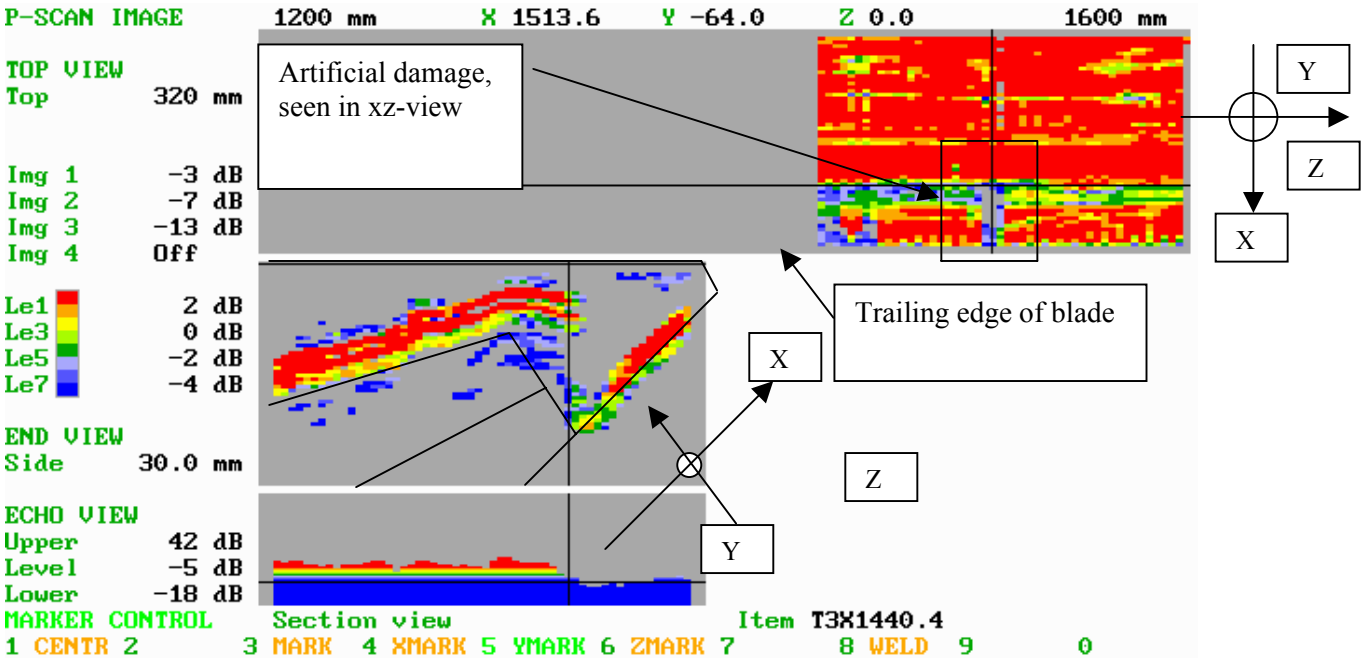

Figure 44. Image showing the result of the ultra sonic inspection of the up-wind surface of the blade after WING 001.

Figure 45. Photo with lines drawn to illustrate the view in the lower part of Figure 44.

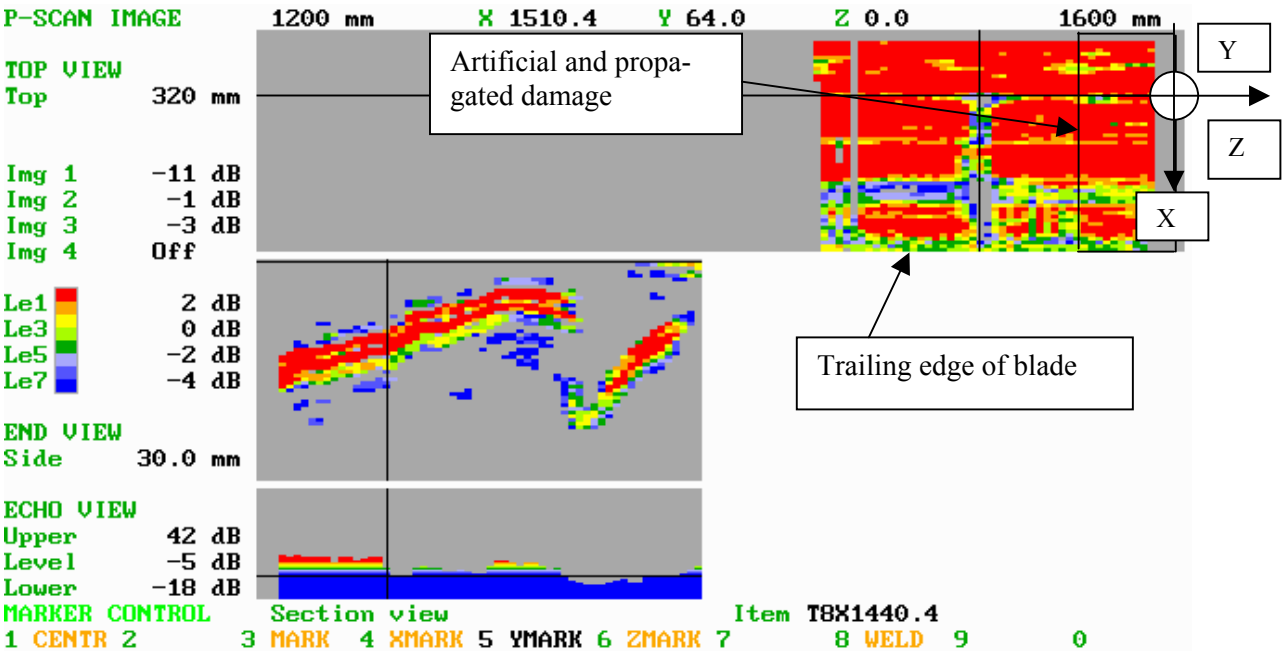

Figure 46. Image showing the result of the ultra sonic inspection of the up-wind surface of the blade after WING 008.

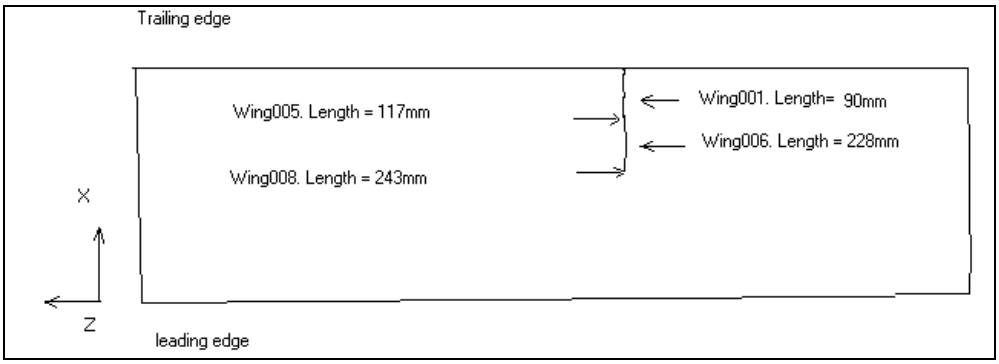

Figure 47. Sketch of propagated damage on down-wind surface after WING008, based on ultrasonic inspections

5.5 X-ray examination of damage no. 1

Methodology

In this case, real time X-ray inspection (known as radioscopy) has been accomplished using a microfocus X-ray source combined with an X-ray image intensifier tube. These units have been mounted on a rail with a specially developed remote controlled positioning unit.

Figure 48. The radioscopy system comprising a compact microfocus source (right) and a real time X-ray image intensifier tube (left), mounted on a rail that in this case was positioned with the help of a crane on the rear edge of the blade.

Figure 49 shows the X-ray image of the down-wind surface of the blade. Note how the crack follows the fibre orientation. This is pronounced at its end where the fibres are orientated at an angle – here the crack veers off sharply. The letter "F" indicates an area where crack forks – the right branch ends after approx. 1.5 cm. The letter "D" indicates an area where crack is diffusely defined, which is probably because the crack is not perpendicular, but runs at an angle to the plan of the blade.

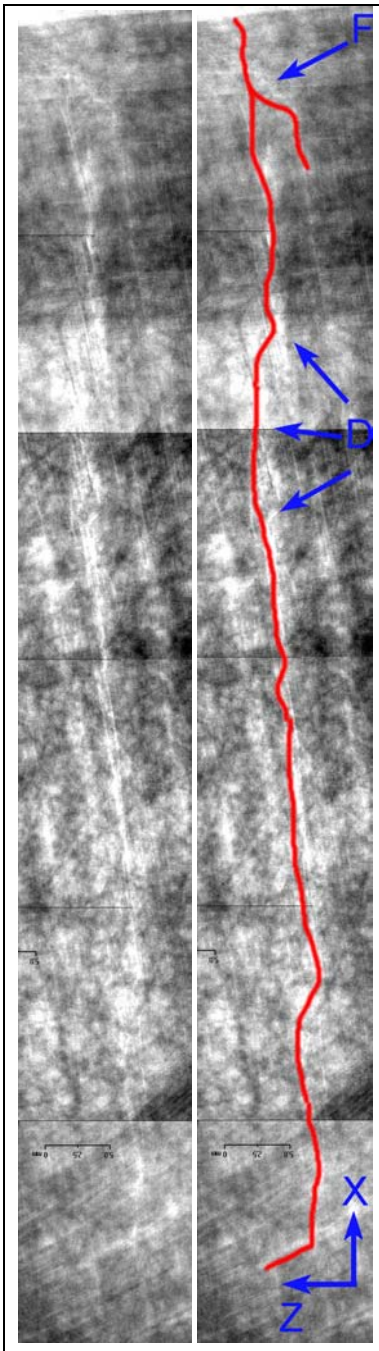

Figure 49. Down-wind X-ray inspection after WING 005

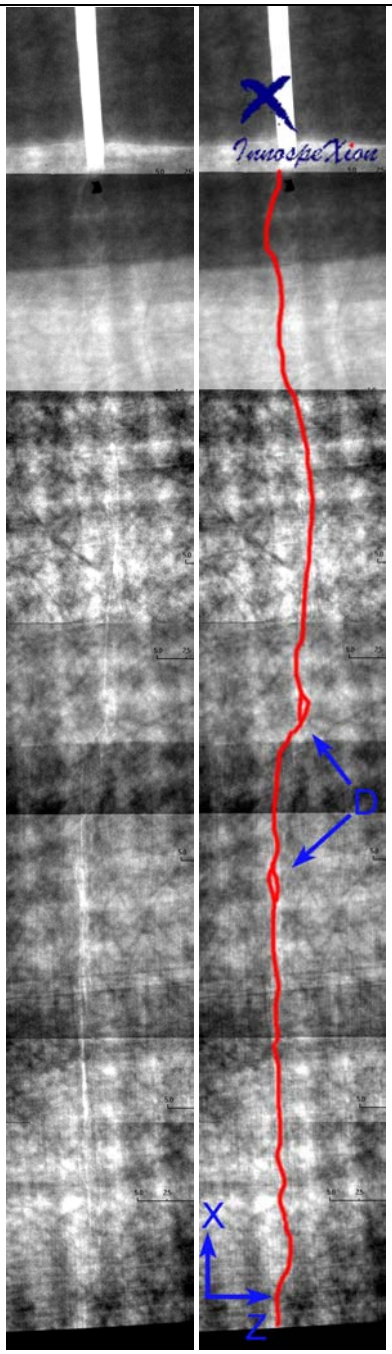

Figure 50. Up-wind X-ray inspection after WING 005

Figure 50 shows the X-ray image of the up-wind surface of the blade. Note how the crack follows the fibre orientation. The crack ends abruptly upon meeting an area of the blade with a sharp increase in thickness. The letter "D" indicates an area where crack is diffusely defined, multiple cracks run through these two areas.

Ref [5] gives a more detailed description of the X-ray inspections.

5.6 Comparison of acoustic emission and strain gauge measurements

The AE results and the strain gauges measurements show good capability in determining the crack propagation and give good visualisation of the speed of crack propagation. The major growth in crack length during WING005 happens in the last third of the test. This is very visible in the change in strain-level in the strain graph in top of Figure 51. In Figure 52 it is visible that the major part of AE-hits appears in the last third of the test.

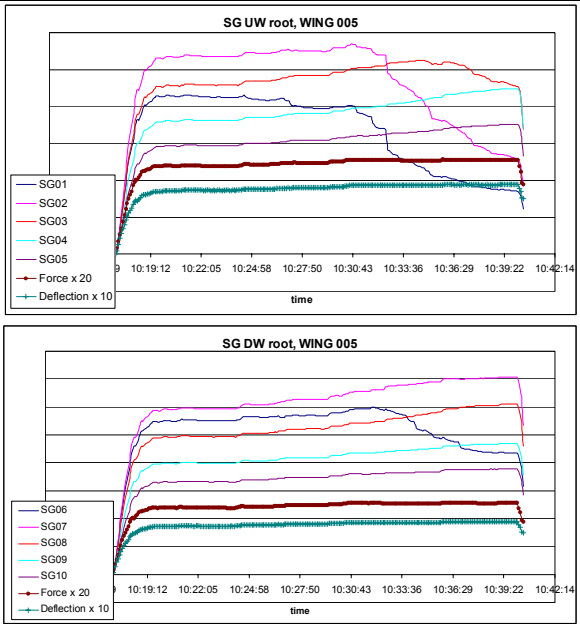

Figure 51. Strain development during WING005

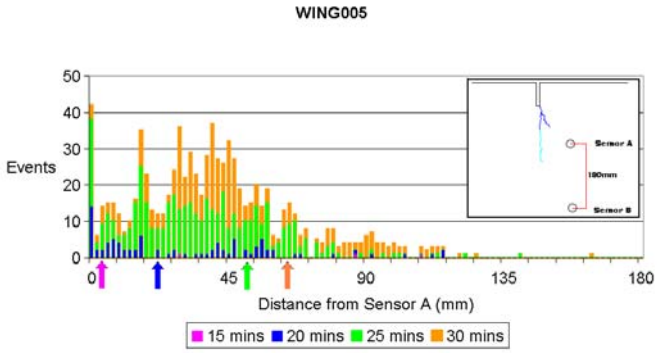

Figure 52. AE-hits vs. time during WING005. Arrows on x-axis shows the distance from crack-tip to sensor A over time.

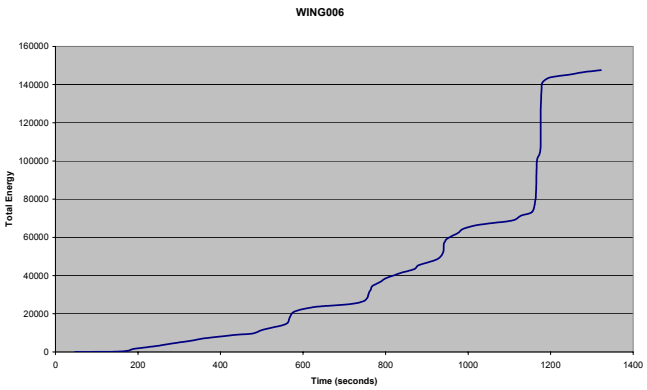

Figure 53. AE-energy measured during WING006

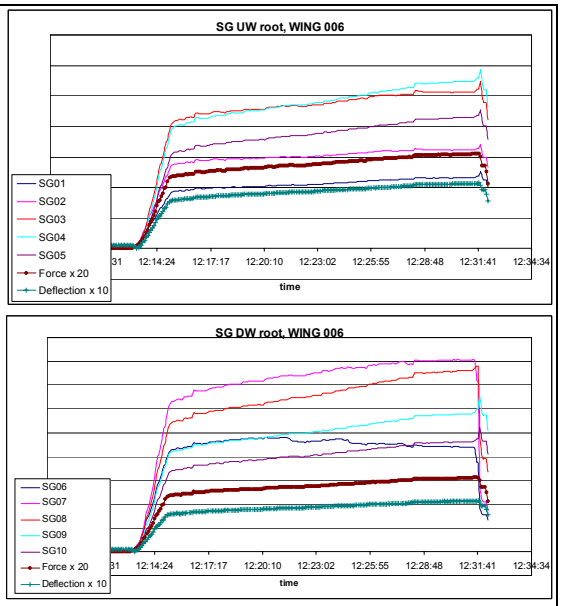

Figure 54. Strain development during WING006

In Figure 53 it is seen that in the very end of test WING006 there is a significant increase in acoustic emission this correlates well with the strain measurements in the lower part of Figure 54. By watching the VCR monitoring of the blade it is seen that the damage propagates very much within a very short period of time in the end of test WING006.

6 Test of damage no. 2

6.1 Overview

The test of the adhesive failure in the trailing edge was difficult to carry out. The reason was the creation method used for this type of damage. Because an angular grinder was used to create the damage, the size of the slot became very wide compared to the remaining part of the trailing edge. This caused the trailing edge to become very soft and easy to buckle where the glue had been removed. While the trailing edge was so easy to buckle it was difficult to control the crack propagation. Reinforcement of the trailing edge was made by clamping on plywood in the area where buckling appeared.

The repetitions in the test of damage no. 2 were numbered as shown in Table 5, here is also seen the damage propagation during each test i.e. the visible elongation of the damage.

Table 5. Test of damage no. 2, test-name and damage propagation measured by visual inspection, by means of VCR, of damage.

test #	**Trailing edge SG1-6 & SG7-12**		
	crack length at start of test	**growth during test**	crack length at stop of test
	mm	**mm**	mm
WING101	0	**0**	0
WING102		**0**	
WING103		**0**	
WING104		**0**	
WING105		**0**	
WING106		**0**	
WING107		**0**	
WING108		**0**	
WING109		**0**	
WING110		**0**	
WING111		**0**	
WING112		**0**	
WING113	0	**0**	
WING114	0	**49**	49
WING115	49	**58**	107
WING116	107	**41**	148
WING117			
WING118	148	**158**	265

Still photos and post-mortem sectioning

Still photos were taken of the damaged blade after some of the tests, see figure Figure 55 to Figure 57.

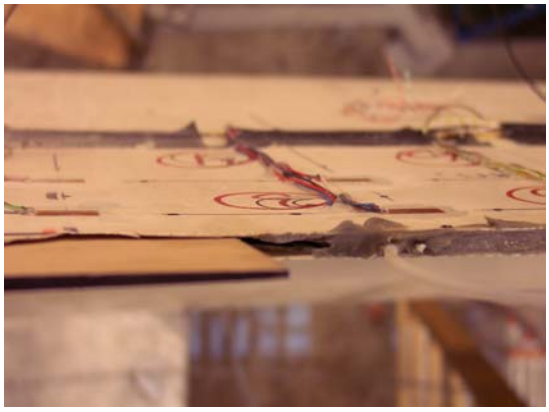

Figure 55. Trailing edge after WING 106

Figure 56. Trailing edge before WING 109

Figure 57. Trailing edge after WING 118

Subsequent to the test sections of the blade were cut out for further examination

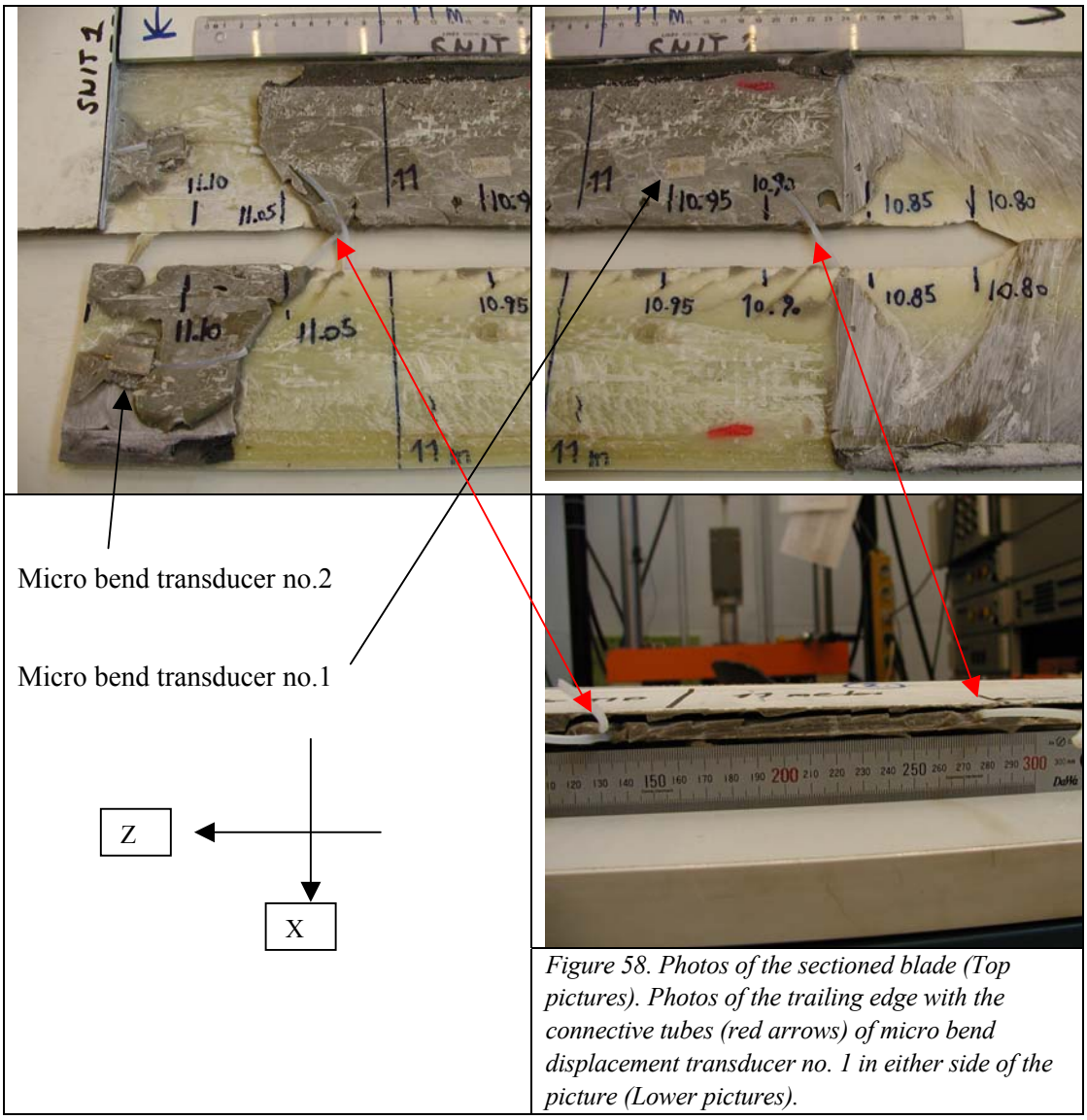

Figure 58. Photos of the sectioned blade (Top pictures). Photos of the trailing edge with the connective tubes (red arrows) of micro bend displacement transducer no. 1 in either side of the picture (Lower pictures).

On these pictures it appears as the damage is propagating in an angel of 30° to 45° relative to the trailing edge and with direction towards the tip. This corresponds very well to the ultrasonic inspections as described in paragraph 6.5.

6.2 Strain gauges results

To measure the strain distribution in the area of the damage, 12 strain gauges were mounted on the blade in the area of damage 2; see Figure 59. The exact positions of the gauge are shown in Figure 60.

On the pictures the tip-end of the blade is towards the left on the page.

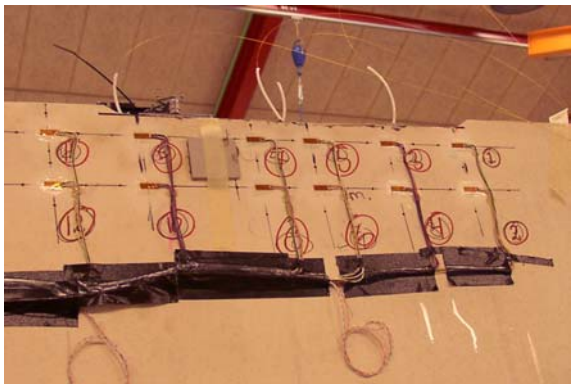

Figure 59. SG-pos. damage 2 Down-wind.

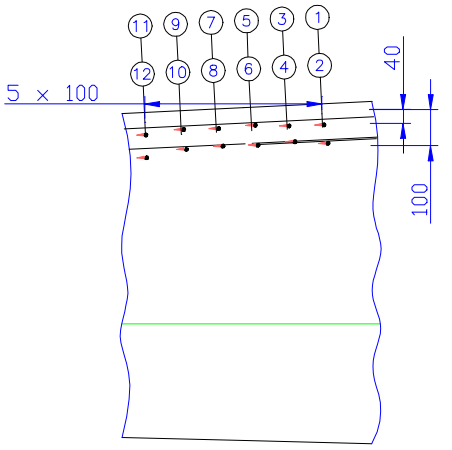

Figure 60. SG-positions damage 2. SG no. 1 & 7 are positioned in a distance of 10.8 metres from root intersection.

As the load was applied to the blade a linear related increase in strain level was measured on all the strain gauges. The relation in strain level between the strain gauges was also linear in correspondence to the distance from the neutral line of the blade. The linearity ruled for tests “WING 101 to “WING 105”. During test “WING 106” the strain level for gauge no. 3 decreased in strain level as the rest of the gauges were still increasing, see *Figure 61*.

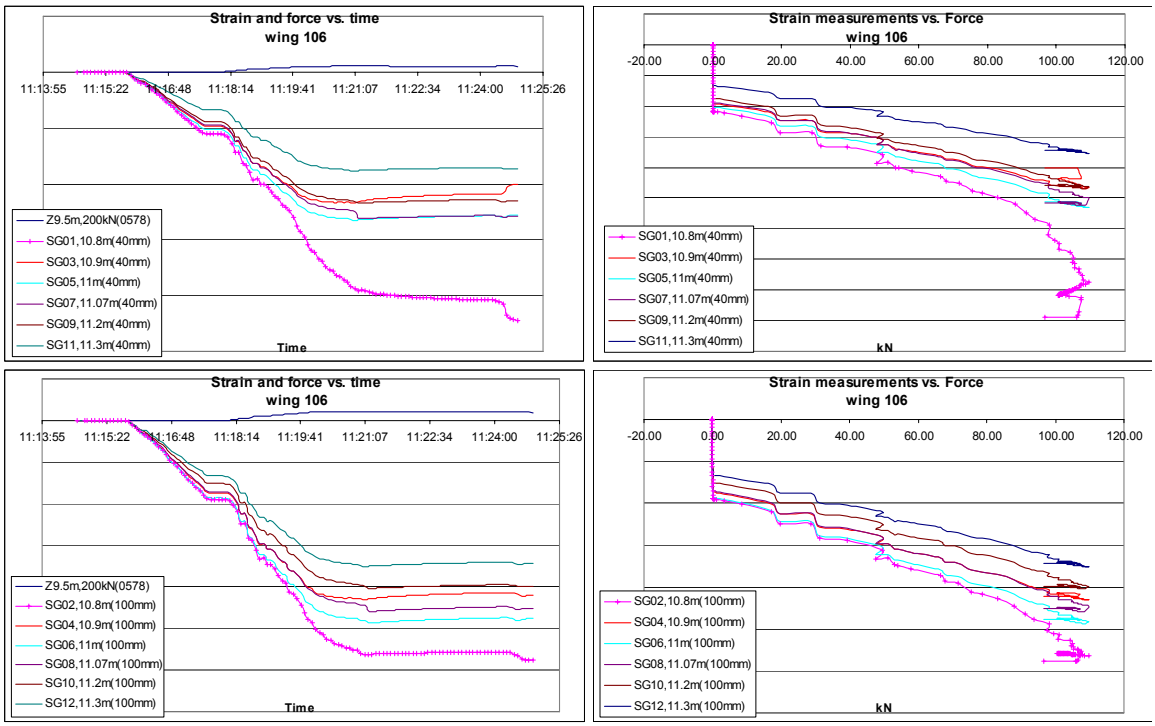

Figure 61. Measured strain, force and deflection during "WING 106"

This indicates buckling which is also very visible on the video. This buckling in the area of gauge no. 3 appeared in all the tests. The change in strain level between single gauges does not correspond to the crack propagation. It is impossible to determine the crack propagation from the strain gauge measurements.

6.3 Acoustic emission results

During series 2 the AE systems were used as an aid to the loading procedure. The onset of acoustic emission was an indication that load had reached a level at which damage was occurring in the structure. AE sensors were also placed at the loading yoke and at the clamped end of the adhesive crack to act as warning sensors; activity here indicated that damage was developing in areas other than those required for the test.

The AE sensors were therefore being used in zonal source location mode during these tests. Attempts to use time of flight measurements to localise the precise extent of the adhesive crack advance were not successful. The reason is that stress wave emission during the loading was not limited to the crack tip. Legitimate sources were present on either side of the crack front (adhesive cracking, fibre bridging, tribology, etc.). In addition to this, buckling of the structure and friction sources from the loading saddle and clamps resulted in too distributed an area of stress wave emission for accurate localisation of the crack front.

6.4 Micro bend displacement transducer results

A lot of tests were carried out without any change in transmittance of the micro bend transducer (the crack front being too far away from the sensor to be detected). Due to the method of creating the artificial damage the trailing edge was very soft where the adhesion had been removed. Therefore it was easy to get the

trailing edge to buckle where the adhesion was removed and difficult to make the damage propagate where the transducers were embedded.

During the first test sequence WING114, there was for the first time a change in the transmittance of the transducer see Figure 62.

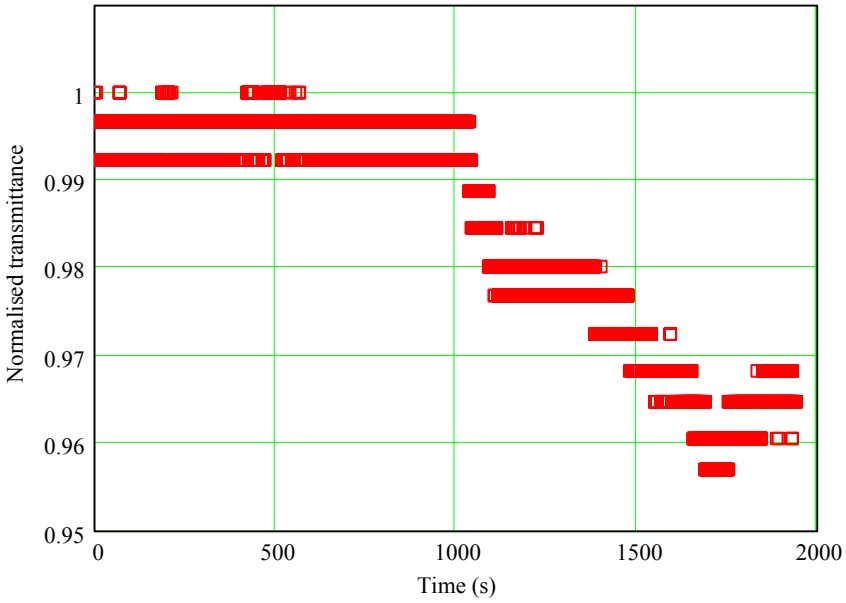

Figure 62. Micro bend displacement transducer measurements during WING114

The first 1000 seconds the load on the tip was increased, the load in the centre yoke was gradually increased and the crack started growing. The deformation of the blade had apparently no impact on the transmittance of the transducer. The transducer started to change transmittance at a time when the transducer is reached by the crack tip. The load was still increased, causing a large crack opening, and a still lower transmittance. After 1700 s the load is gradually removed. The entire load was removed after 1900 s. Figure 62 shows that the transducer only partially resumes its initial transmittance. A permanent crack opening is apparently created.

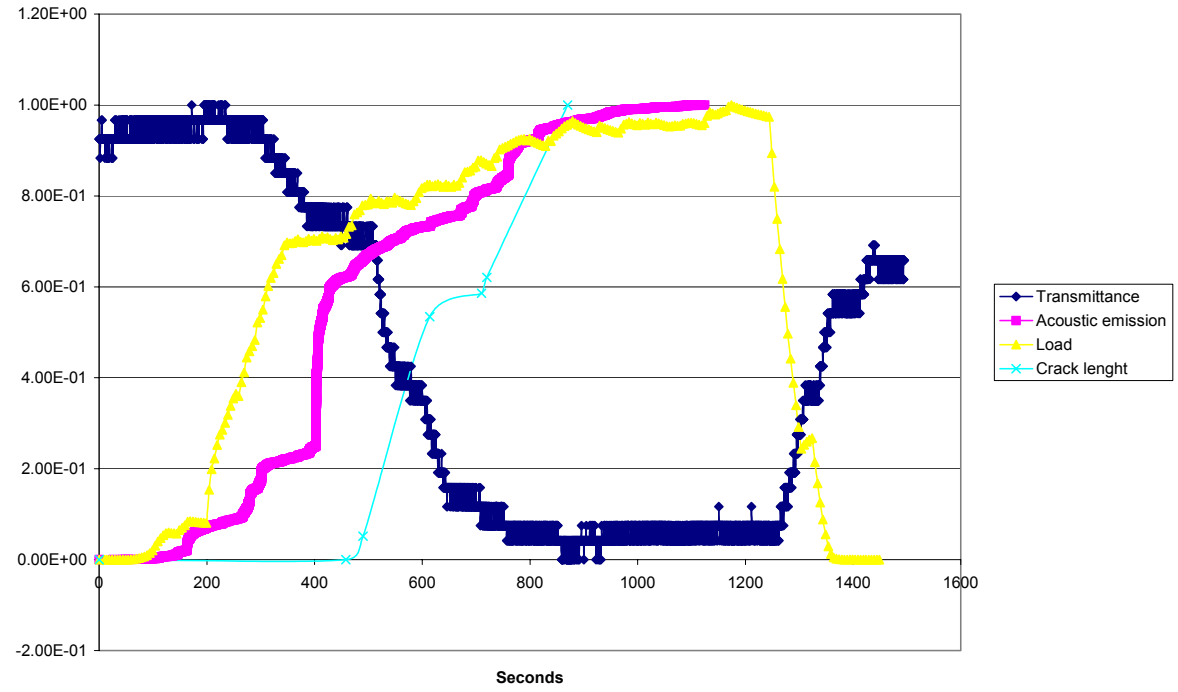

Figure 63. Transmittance of micro bend transducer correlated with normalised values of force, acoustic emission energy and crack propagation during WING115.

In WING115, the load was still more increased with a 10 % decrease in transmittance as a consequence, see Figure 63. The load was increasing until 1200 s, but apparently the deformation of the sensor reached a maximum. After 1200 s the load is removed and the transducer resumes most of its original transmittance.

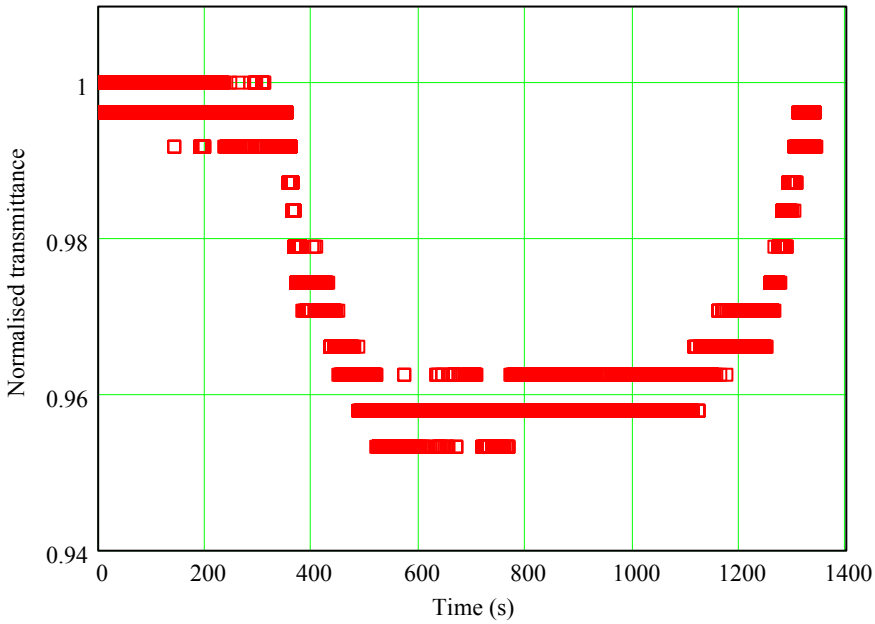

Figure 64. Micro bend transducer signal during WING116

To increase the bending moment in the damaged area the support was repositioned and new load sequence was carried out. As

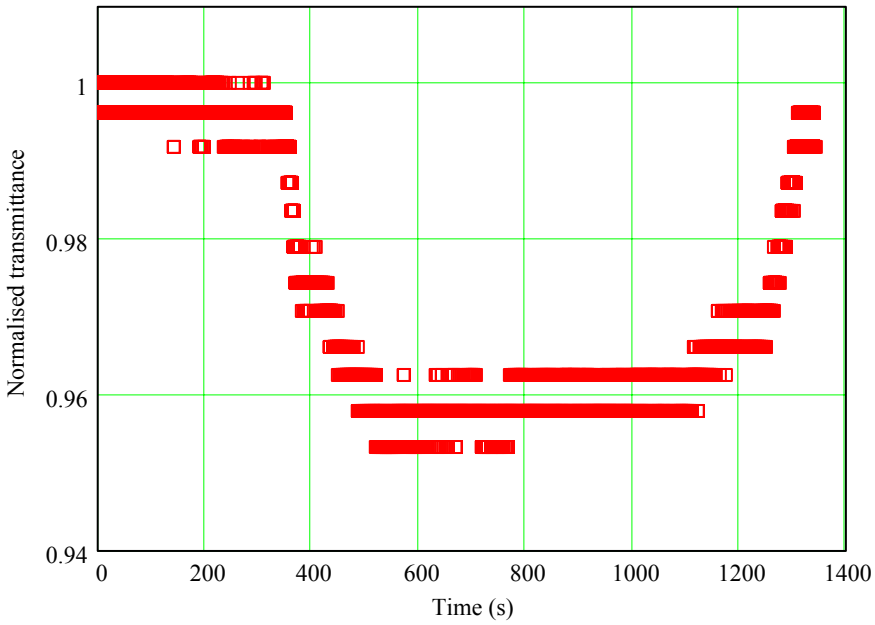

Figure 64 shows, the transmittance decreases once more, but only a few percent, even though the crack with almost certainty passed the transducer, and the gap was large. The transmittance did not fall to zero, as expected for a crack width larger that 200 um.

The blade was unloaded and the supporting devices were repositioned, and a new test WING117 was carried out.

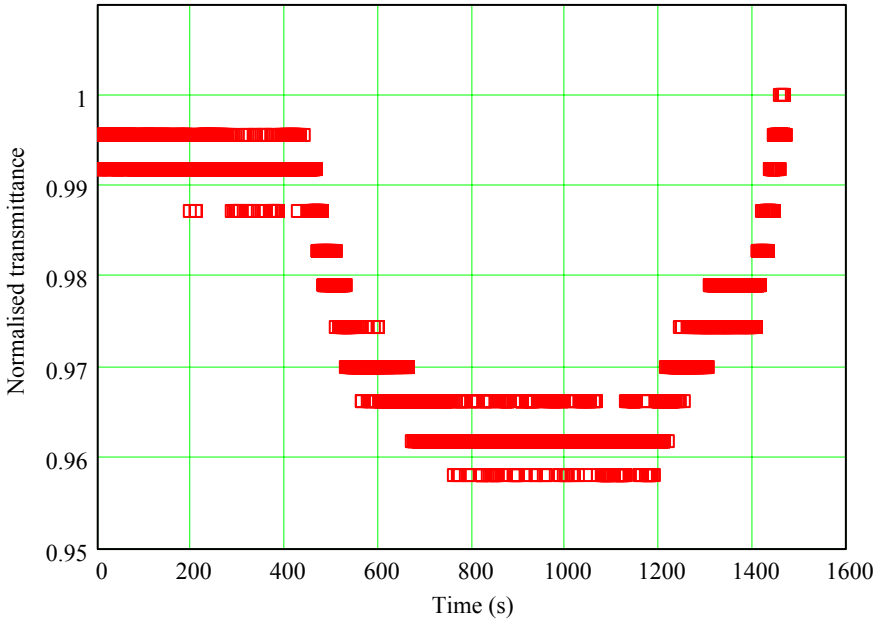

Figure 65. Micro bend transducer signal during WING117

This new test was apparently a repetition of the test before. There was a decrease in transmittance until a certain point. The crack had now passed the transducer and the crack was at maximum load several mm wide. A blade was inserted in to the crack, at the location of the transducer, and pushed to the bottom of the adhesive region. There was no detectable contact between the transducer and one of the shells. The crack was in the interface between one of the shells and the adhesive layer and the transducer was fully contained in the adhesive. The surface, which initially was glued to the shell, was now almost completely loosened. This conclusion was reached after direct visual inspection, through the crack opening, and by use of a blade. The change of transmittance indicates that there was some contact, but maybe only through a number of loosened glass - fibres, that had been torn out of the fibreglass composite.

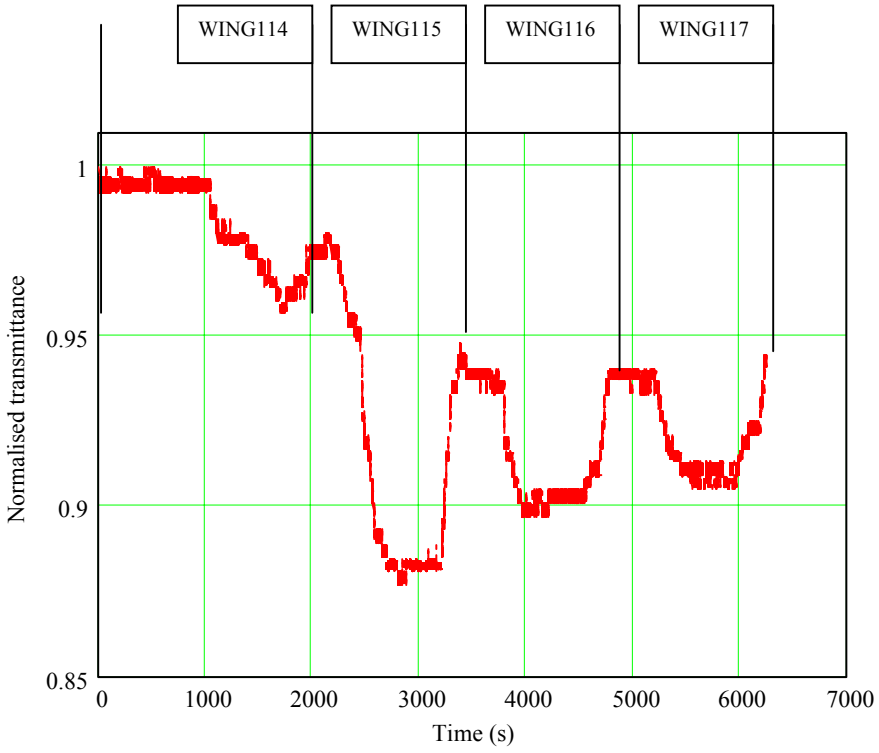

Figure 66. Micro bend transducer signal during WING114- WING117.

The variation of the transmittance through all 4 tests is displayed in Figure 66. The normalised transmittance is here defined as the ratio between the power and the largest power in all four series. The maximum decrease in transmittance was 12.3%, which corresponds to a deformation of the transducer of 12.3%/(0.5 %/um) = 25 um. The first deformation is apparently irreversible and the initial transmittance was not reached again. This agrees well with the circumstance that the transducer permanently loosened most of its contact to one of the shells.

After test WING117 the crack had passed transducer A and this transducer was not expected to show any further change in transmittance. The light source and the detector were instead coupled to the optical fibres of transducer B.

A wooden wedge was hammered into the notch and the crack advanced quickly.

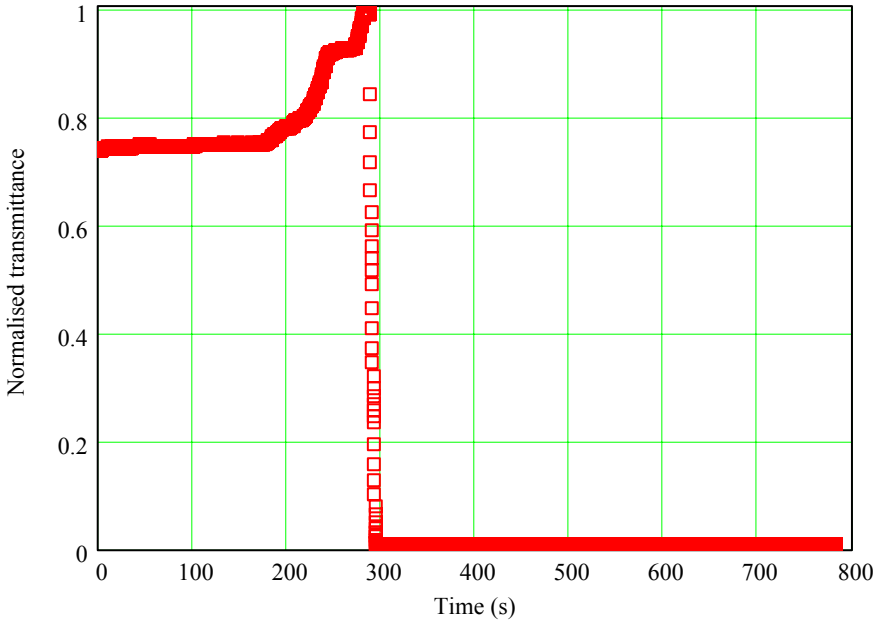

Figure 67. Change in transmittance during WING118.

As Figure 67 shows there is a small increase in transmittance, after which the transmittance drops to zero over a short period of time. Hereafter the wedge is removed and the load on the yoke nearest the tip is removed. The movement of the wedge and the unloading of the blade did not change the transmittance. The fiber is probably squeezed into two or more pieces inside the transducer, because all will be carried by the optical fiber, when the deformation of the transducer is more than 200 um.

Conclusions regarding fibre-optics sensor on full-scale test

Two transducers were mounted in the trailing edge of a wind turbine blade in two different ways.

1) One transducer was simply inserted into a notch grinded into the edge. Adhesive was injected into the notch to refill the notch itself and the small space between the notch and transducer to ensure a proper adhesion between the transducer and the surfaces of the notch (the inner surfaces of the shell). As a crack passed the transducer it changed transmittance by 12.3%. This relatively small change in transmittance indicates that the transducer did not pick up all the relative displacement of the shells. Inspection showed that the transducer lost its contact to one of the shells.

2) The second transducer was mounted with direct attachment to the outer surfaces of the shells. The direct connection was obtained through a circular hole in both outer surfaces. The two holes were filled with adhesive and covered with a square shaped piece of fibre-glass. Unfortunately there was not sufficient time to make the crack pass transducer B, by gradually increasing the load on the yoke nearest the root of the blade. Instead, the crack was evolved by hammering a wedge into the notch. The transducer responded with a 100% change in transmittance. The transducer turned out to be

mounted so firmly, that the fibre inside the transducer was not only deformed, it was simply crushed.

6.5 Ultra-sonic examination of damage

After each test ultra sonic inspections (US-I) were made of the damage to have another estimate of damage size. To have a basis for the ultra-sonic determination of the damage propagation two ultra-sonic tests were made on the blade before the tests of the blade were carried out. The first US-I was made when the undamaged blade was mounted on the test rig and the second US-I was made after the artificial damage was made on the blade.

The initial inspection of the blade was made in the area from 11600 mm from root intersection and till 14000 mm. The inspected area was separated in sections of 400 mm in longitudinal direction and all sections had a size of 320 mm in direction perpendicular to the trailing edge, measured from the trailing edge. The results from the ultrasonic inspections are further described in [Ref. 6].

Table 6. Table showing ultra sonic results for inspection of the trailing edge joint on up-wind surface.

Date	Time	Test	File-name	**Comments to scanning-results.**
10/01.02	16:22		T1-a.1	Reference examination. OK.
23/01.02	11:17		T2a-X600	Examination of torn out fibres after grinding of notch. OK.
24/01.02	09:13		T3a-X600	Blade has been cut from cusor towards root-end of blade
24/01.02	11:57	WING 106	T4a-X600	Additional elongation of damage towards root-end of blade, made by use of saw.
24/01.02	14:22	WING 107	T5a-X600	Propagation of damage, app. 10 mm towards tip-end of blade.
24/01.02	15:15	WING 108	T6a-X600	Additional propagation of damage, app. 20 mm towards tip-end of blade.
25/01.02	08:14	WING 113	T7a-X600	Further damage propagation, app. 13 mm.
25/01.02	10:23	WING 114	T8a-X600	Further damage propagation, app. 25 mm.
25/01.02	11:56	WING 115	T9a-X600	Further damage propagation, app. 30 mm.
25/01.02	14:08	WING 117	T10aX600	Further damage propagation into area of optic fibre plug, impossible to test this area.
28/01.02	9:33	WING 118	T11aX600	Further damage propagation out of area of optic fibre plug, impossible to test this area.

In the first three scans, after load has been applied, (File T3A-X600- T4A-x600 and file T5A-x600) the front of the crack, develops from being curved with a tendency to arrow shape, to have a 45° line ending on the trailing edge of the blade.

In the next three scans, (File T6A-x600.- T7A-x600.- T8A-x600.) the shape of, the front of the crack, goes back to be a curved arrow shape.

In the next scan, (File T9A-x600) the shape of, the front of the crack, develops to a 45° line. This time it ends on the inner side of the adhesively bonded area.

In paragraph 6.1 pictures of the post-mortem sectioning shows the described change in crack propagation direction. The shapes of, the front of the crack, could not be determined in the last two scans.

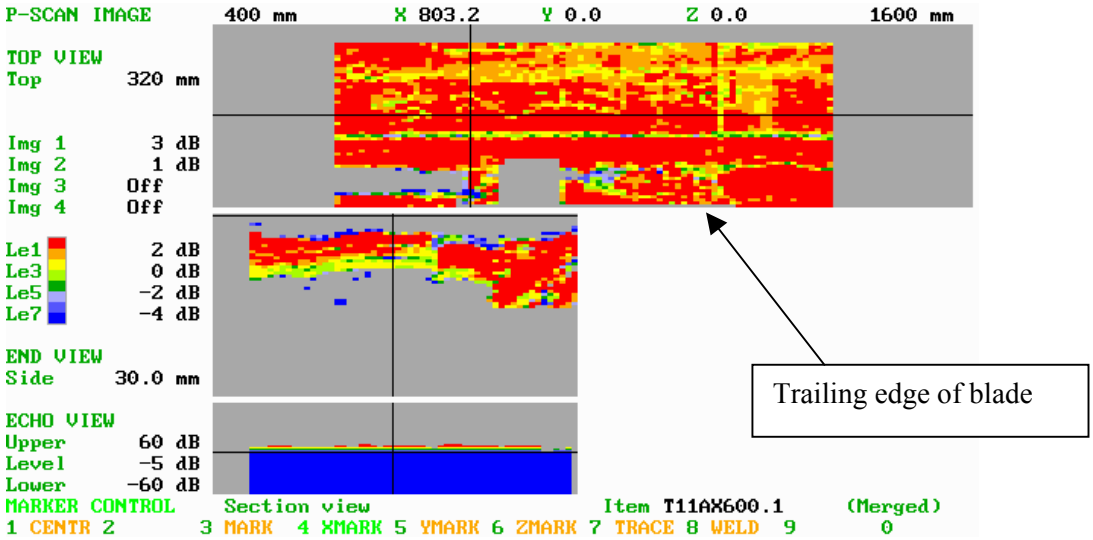

Figure 68. Image showing the result of the ultra sonic inspection of the up-wind surface of the blade after WING 118.

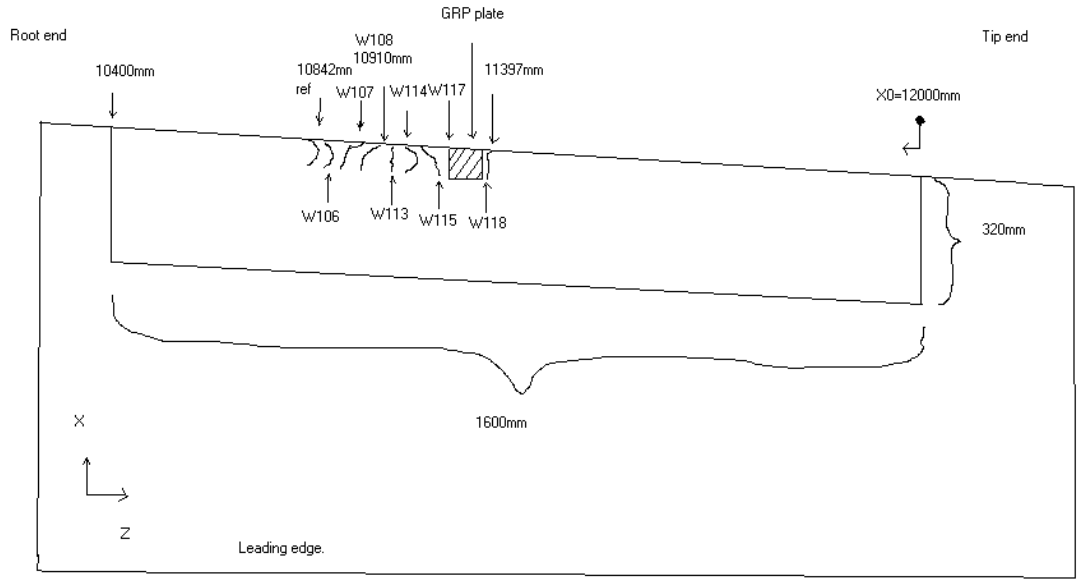

Figure 69. Sketch of damage propagation based on the ultrasonic inspections

VCR monitoring of damage no. 2

During each of the tests of damage no. 2 a video camera was used to survey the propagation in the damage. The camera was positioned over the trailing edge directed towards the trailing edge. When comparing the VCR with the post mortem sectioning it has been possible to estimate the crack propagation in the tests. Test no. 114, 115 and 118 were the tests where the measurements from the

optic micro bend displacement transducer showed the highest changes. Crack propagation for these three tests are described in 0.

Table 7. Crack propagation during test 114, 115 and 118.

Test no.	Time (00:00:00 h:m:s at test start)	Crack length in mm	Crack position as it appears on VCR, measured in mm in Z-direction
WING 114	00:00:00	0	10870
	00:14:50	10	10880
	00:17:05	35	10905
	00:18:05	37	10907
	00:24:50	49	10919
WING 115	00:00:00	49	10919
	00:07:38	49	10919
	00:08:10	52	10922
	00:10:14	80	10950
	00:11:50	83	10953
	00:12:00	85	10955
	00:14:30	107	10977
WING 118	00:00:00	148	11018
	00:15:25	190	11060
	00:15:52	209	11079
	00:16:04	232	11102
	00:16:22	265	11135

If the crack propagation as it appears on the VCR is related to the results from the ultrasonic inspection there is a minor difference in the results. The explanation for this can be that the visible crack tip is at the trailing edge an there might be a shift, or not-linear, propagation in the crack tip through the adhesion. Which is also sketched in Figure 69.

7 Conclusion

Strain gauges: By use of strain gauges it is possible to measure changes in strain distribution caused by propagating damages. The necessary number of gauges depends on the size of damage the system is monitoring.

Acoustic emission: The acoustic emission system is very capable of detecting even minor crack propagation. The position and severity of damage source events has been successfully determined using both zonal and linear time-of-flight localisation arrays.

The optic fibre micro-bend displacement transducer is capable of determining crack propagation in adhesive joints (and possible also delaminations). It is at least useable for determining crack size corresponding to the distance between each transducer. The transducer signal transmittance is gradually decreasing when the transducer is passed by the crack front and the crack advances. Potentially, the value of the crack opening may be used for estimation of a minimum crack extension, with a resolution better than the distance between the transducers. It is very important that the transducer remains attached to the separating surfaces because the crack is detected by the relative displacement.

Both the X-ray and the ultra sonic equipment are capable of locating the damage and determining the size of the damage. The ultra sonic system is well suited for determining the size and location of failure in the adhesive joint and most likely also delaminating failures.

For the laminate damage (the notch in the trailing edge) the resolution of the ultra sonic system is too low to give an accurate position of the crack tip. For this damage type the X-ray technique proved to be very versatile. Used in combination, ultrasonic scanning and X-ray inspection are strong NDT-tool for damage detection and localisation in wind turbine blades.

In general, very satisfying agreement were found between the information on damage size and location by sensors, NDT-techniques and post-mortem analysis.

8 Contacts

- Peter Sendrup, DELTA, Danish Electronics, Light & Acoustics. pse@delta.dk, Optic fibre microbending displacement transducer measurements
- Jens Rusborg FORCE Technology. jer@force.dk, Ultra sonic inspections of blade.
- Jørgen Rheinländer, Innospexion Aps.jr@innospexion.dk, X-ray inspections of blade.
- Jørgen D. Vestergaard, LM Glasfiber A/S. jdv@lm.dk, Providing blade for project.
- Lars Lading, Sensor Technology Center A/S. ll@sensortec.dk, Cost Benefit analysis and consultancy on sensors.
- Malcolm McGugan, Risø National Laboratory malcolm.mcgugan@risoe.dk, Acoustic emission measurements.
- Christian P. Debel, Risø National Laboratory, c.p.debel@risoe.dk, Post mortem sectioning and inspection of damaged blade
- Ole J. D. Kristensen, Risø National Laboratory, The Sparkaer Centre, ole.jesper.dahl.kristensen@risoe.dk, Test of blade, SG measurements.
- Bent F. Sørensen, Risø National Laboratory, bent.soerensen@risoe.dk, Materials Research and project management.

Figure 70. Test-crew for damage no. 1, from left: Jørgen Rheinländer, Peter P. Debel, Bent F. Sørensen, Malcolm McGugan, Jens Rusborg, Ole J.D. Kristensen, Jan Andersen, Christian P. Debel

Figure 71. Test-crew for damage no. 2, from left: Per Nielsen, Bent F. Sørensen, Peter Lind, Anders R. Vestergaard, Malcolm McGugan, Jan Andersen, Peter Sendrup.

9 References

[1] Sørensen, B. F.; Lading, L.; Sendrup, P.; McGugan, M.; Debel, C. P.; Kristensen, O. J. D.; Larsen, G.; Hansen, A. M.; Rheinländer, J.; Rusborg, J.; and Vestergaaard, J. D.; (2002) "Fundamentals for remote structural health monitoring of wind turbine blades – a pre-project" Risø-R-1336(EN). Risø National Laboratory, Denmark

[2] Hedner, G. (1978), "Formelsamling i Hållfastehslära", Publikation nr 104, Department of Solid Mechanics, Royal Institute of Technology, Stockholm, p. 316

[3] Hutchinson, J. W., and Suo, Z. (1992), "Mixed mode cracking in layered materials", in Advanced in Applied Mechanics, Vol. 29 (Ed. J. W. Hutchinson and T. Y. Wu), Academic Press, Inc., Boston, pp. 63-191

[4] Sendrup, P. (2002) "Fiber sensor for damage detection in wind turbine blades". DELTA, Danish Electronics, Light & Acoustics.

[5] Rheinländer, J and Jagd, M. (2002) "Elkraft PSO Projekt, Grundlag for fjernovervågning af vindmøllers tilstand". InnospeXion Aps

[6] Rusborg, J. (2002) "4.3.2 Ultrasonic examination results". FORCE Technology

[7] Rusborg, J. and Nielsen, P. (2002) "5.3.2 Ultrasonic examination results". FORCE Technology

Bibliographic Data Sheet **Risø-R-1333(EN)**

Title and authors

Fundamentals for Remote Structural Health Monitoring of Wind Turbine Blades - a Preproject Annex E - Full-Scale Test of Wind Turbine Blade, Using Sensors and NDT

Ole J. D. Kristensen, Malcolm McGugan, Peter Sendrup,
Jørgen Rheinländer, Jens Rusborg, Anders M. Hansen,
Christian P. Debel, Bent F. Sørensen

ISBN	ISSN
87-550-3034-3 87-550-3035-1(Internet)	0106-2840

Department or group	Date
Wind Energy Department	May 2002

Groups own reg. number(s)

Sponsorship	Project/contract No(s)
Elkraft System	Bro-91.055 (FU1102)

Pages	Tables	Illustrations	References
65	7	71	7

Abstract (max. 2000 characters)

A 19.1 metre wind turbine blade was subjected to static tests. The purpose of the test series was to verify the abilities of different types of sensors to detect damage in wind turbine blades. Prior to each of the static test-series an artificial damage was made on the blade. The damage made for each test-series was surveyed during each series by acoustic emission, fiber optic micro bend displacement transducers and strain gauges. The propagation of the damage was determined by use of ultra sonic and X-ray surveillance during stops in the test-series. By use of acoustic emission it was possible to measure damage propagation before the propagation was of visible size. By use of fiber optic micro bend displacement transducers and strain gauges it was possible to measure minor damage propagation. By use of both ultra sonic, and X-ray NDT-equipment it were possible to determine the size of propagated damage.

Descriptors INIS/EDB

ACOUSTIC EMISSION TESTING; DAMAGE; FIBER OPTICS;
INDUSTRIAL RADIOGRAPHY; MECHANICAL TESTS; REMOTE SENSING;
STRAIN GAGES; TRANSDUCERS; TURBINE BLADES;
ULTRASONIC TESTING; WIND TURBINES

RISØ

Mission

To promote an innovative and environmentally sustainable technological development within the areas of energy, industrial technology and bioproduction through research, innovation and advisory services.

Vision

Risø's research shall **extend the boundaries** for the understanding of nature's processes and interactions right down to the molecular nanoscale.
The results obtained shall **set new trends** for the development of sustainable technologies within the fields of energy, industrial technology and biotechnology.
The efforts made **shall benefit** Danish society and lead to the development of new multi-billion industries.

ISBN 87-550-3034-3
ISBN 87-550-3035-1 (Internet)
ISSN 0106-2840

Risø National Laboratory
Information Service Department
P.O. Box 49
DK-4000 Roskilde
Denmark
Telephone +45 4677 4004
risoe@risoe.dk
Fax +45 4677 4013
Website www.risoe.dk